Shaler: insitu analysis of a fluvial sedimentary deposit on Mars

Ralph E. Milliken, Michelle Minitti, Marisa Palucis, Melissa Rice, Scott K. Rowland, Juergen Schieber, Kathryn M. Stack, Dawn Y. Sumner, Roger C. Wiens, Rebecca M. E. Williams, et al.

Shaler: *in situ* analysis of a fluvial sedimentary deposit on Mars

LAUREN A. EDGAR[1] , SANJEEV GUPTA[2], DAVID M. RUBIN[3], KEVIN W. LEWIS[4], GARY A. KOCUREK[5], RYAN B. ANDERSON[1], JAMES F. BELL III[6], GILLES DROMART[7], KENNETH S. EDGETT[8], JOHN P. GROTZINGER[9], CRAIG HARDGROVE[6], LINDA C. KAH[10], RICHARD LEVEILLE[11], MICHAEL C. MALIN[8], NICOLAS MANGOLD[12], RALPH E. MILLIKEN[13], MICHELLE MINITTI[14], MARISA PALUCIS[9], MELISSA RICE[15], SCOTT K. ROWLAND[16], JUERGEN SCHIEBER[17], KATHRYN M. STACK[18], DAWN Y. SUMNER[19], ROGER C. WIENS[20], REBECCA M. E. WILLIAMS[14] and AMY J. WILLIAMS[21]

[1]*U.S. Geological Survey, Astrogeology Science Center, 2255 N. Gemini Dr., Flagstaff, AZ 86001, USA (E-mail: ledgar@usgs.gov)*
[2]*Department of Earth Science and Engineering, Imperial College, London, SW7 2AZ, UK*
[3] *Department of Earth & Planetary Sciences, University of California, 1156 High Street, Santa Cruz, CA 95064, USA*
[4]*Department of Earth and Planetary Sciences, Johns Hopkins University, 301 Olin Hall, 3400 N. Charles Street, Baltimore, MD 21218, USA*
[5]*Department of Geological Sciences, Jackson School of Geosciences, University of Texas at Austin, 2305 Speedway Stop C1160, Austin, TX 78712-1692, USA*
[6]*School of Earth and Space Exploration, Arizona State University, Tempe, AZ 85281, USA*
[7]*Laboratoire de Geologié de Lyon, Université de Lyon, 69364, Lyon, France*
[8]*Malin Space Science Systems, 5880 Pacific Center Boulevard, San Diego, CA 92121, USA*
[9]*Division of Geological and Planetary Sciences, California Institute of Technology, 1200 East California Boulevard, Pasadena, CA 91125, USA*
[10]*Department of Earth and Planetary Sciences, University of Tennessee, Knoxville, TN 37996-1410, USA*
[11]*Department of Earth & Planetary Sciences, MGill University, Montreal, Quebec, Canada*
[12]*Laboratoire de Planétologie et Géodynamique, Université de Nantes, 44322, Nantes, France*
[13]*Department of Geological Sciences, Brown University, Providence, RI 02912, USA*
[14]*Planetary Science Institute, 1700 East Fort Lowell Road #106, Tucson, AZ 85719, USA*
[15]*College of Science and Engineering, Western Washington University, Bellingham, WA 98225-9160, USA*
[16]*School of Ocean and Earth Science and Technology, University of Hawaii at Manoa, Honolulu, HI 96822, USA*
[17]*Department of Geological Sciences, Indiana University, 1001 East 10th Street, Bloomington, IN 47405-1405, USA*
[18]*Jet Propulsion Laboratory, California Institute of Technology and NASA Astrobiology Institute, 4800 Oak Grove Drive, Pasadena, CA 91109, USA*
[19]*UC Davis, Earth and Planetary Sciences, Davis, CA 95616, USA*
[20]*Los Alamos National Laboratory, Los Alamos, NM 87545, USA*
[21]*Department of Physics, Astronomy and Geosciences, Towson University, Towson, MD 21252, USA*

ABSTRACT

This paper characterizes the detailed sedimentology of a fluvial sandbody on Mars for the first time and interprets its depositional processes and palaeo-environmental setting. Despite numerous orbital observations of fluvial landforms on the surface of Mars, ground-based characterization of the sedimentology of such fluvial deposits has not previously been possible. Results from the NASA Mars Science Laboratory *Curiosity* rover provide an opportunity to reconstruct at fine scale the sedimentary architecture and palaeomorphology of a fluvial environment on Mars. This work describes the grain size, texture and sedimentary facies of the Shaler outcrop, reconstructs the bedding architecture, and analyses cross-stratification to determine palaeocurrents. On the basis of bedset geometry and inclination, grain-size distribution and bedform migration direction, this study concludes that the Shaler outcrop probably records the accretion of a fluvial barform. The majority of the outcrop consists of large-scale trough cross-bedding of coarse sand and granules. Palaeocurrent analyses and bedform reconstruction indicate that the beds were deposited by bedforms that migrated towards the north-east, across the surface of a bar that migrated south-east. Stacked cosets of dune cross-bedding suggest aggradation of multiple bedforms, which provides evidence for short periods of sustained flow during Shaler deposition. However, local evidence for aeolian reworking and the presence of potential desiccation cracks within the outcrop suggest that fluvial deposition may have been intermittent. The uppermost strata at Shaler are distinct in terms of texture and chemistry and are inferred to record deposition from a different sediment dispersal system with a contrasting provenance. The outcrop as a whole is a testament to the availability of liquid water on the surface of Mars in its early history.

Keywords Fluvial, Gale crater, Mars, sedimentology, stratigraphy.

INTRODUCTION

Has the surface of Mars ever experienced sustained fluvial flows? Orbital observations over the past four decades reveal a rich record of erosional and depositional landforms that are inferred to have formed by fluvial processes (Malin & Edgett, 2003; Irwin *et al.*, 2005; Moore & Howard, 2005; Burr *et al.*, 2010; Goddard *et al.*, 2014; Baker *et al.*, 2015). Perhaps most exciting has been the recognition of sedimentary rock deposits that, from their preserved morphology, imply deposition by ancient river flows (Malin & Edgett, 2003; Grotzinger *et al.*, 2011; Rice *et al.*, 2011; Kite *et al.*, 2015). Despite these observations, the absence of detailed records of the sedimentology of such fluvial landforms from existing orbital images means that interpretation of depositional processes and palaeoenvironments is commonly equivocal or simplistic by comparison with terrestrial examples; this is because the bed-scale sedimentary textures and geometries that are typically used to infer fluvial depositional environments on Earth cannot be documented rigorously using orbital imagery. Moreover, from orbital images alone, it remains difficult to reconstruct the fine-scale evolution of sedimentary environments and their spatial distribution. On Earth, studies of ancient fluvial systems involve analysis of metre-scale fluvial sedimentary deposits in outcrop. Analytical techniques include grain-size and textural analysis, identification and interpretation of sedimentary facies, and characterization of the sedimentary architecture of fluvial sedimentary rocks. Integration of such methods enables reconstruction of the morphodynamics of ancient terrestrial fluvial systems.

The *in situ* exploration of sedimentary rocks in Gale crater by the NASA Mars Science Laboratory (MSL) *Curiosity* rover, however, is transforming current understanding of the Martian sedimentary record through documentation of

sedimentary features at outcrop geology scale (Grotzinger *et al.*, 2014). The goal of the *Curiosity* rover mission is to assess evidence for ancient habitable environments. Shortly after landing in Gale crater, the *Curiosity* team discovered patches of conglomerate bedrock comprising cemented rounded pebbles that are interpreted as being of fluvial origin (Williams *et al.*, 2013). Subsequently, *Curiosity* documented a coarsening-upward sedimentary succession in the Yellowknife Bay formation that is interpreted to record progradation of a sandy fluvial system into an ancient, probably shallow, lake (Grotzinger *et al.*, 2014). Detailed analyses of the lacustrine deposits at the base of the Yellowknife Bay formation revealed the first habitable environment investigated by the rover (Grotzinger *et al.*, 2014).

Within the Yellowknife Bay formation, the Glenelg member contains a well-exposed distinct outcrop – informally known as 'Shaler'. [Note that the names used for rock and soil targets studied by *Curiosity* are derived from rock formations on Earth. Prior to landing, the ellipse and nearby areas were divided into square quadrangles (1·5 km on a side) and each quadrangle was assigned a name of a town with a population of less than 100 000 people. As Curiosity investigates rock targets within a quadrangle, names are informally assigned to the targets that correspond to geological formations and features from that

town on Earth. Shaler is part of the Yellowknife Bay quadrangle, named after the town in northern Canada.] This outcrop contains a remarkably rich diversity of sedimentary structures and geometries, which is interpreted below to have been formed by fluvial processes. The analysis of Shaler represents the first opportunity to perform a detailed sedimentological investigation of a fluvial sedimentary deposit on Mars. The aim of this paper is to characterize the sedimentology of the Shaler outcrop and to interpret it in terms of depositional processes and palaeoenvironmental setting. Specific research objectives are as follows: (i) document the sedimentary facies at the Shaler outcrop; (ii) describe the spatial variation in facies and sedimentary architecture; (iii) describe palaeoflow patterns determined from sedimentary structures; (iv) reconstruct the palaeoenvironment; and (v) discuss the implications for Martian climate and habitability. This analysis reveals how rover investigations can be used to reconstruct and interpret fine-scale sedimentary morphologies on Mars.

GEOLOGICAL SETTING

Curiosity landed in Gale crater, a *ca* 150 km diameter impact crater located near the equator (137·7°E, 5·44°S). Gale lies on the crustal dichotomy, between the cratered southern highlands

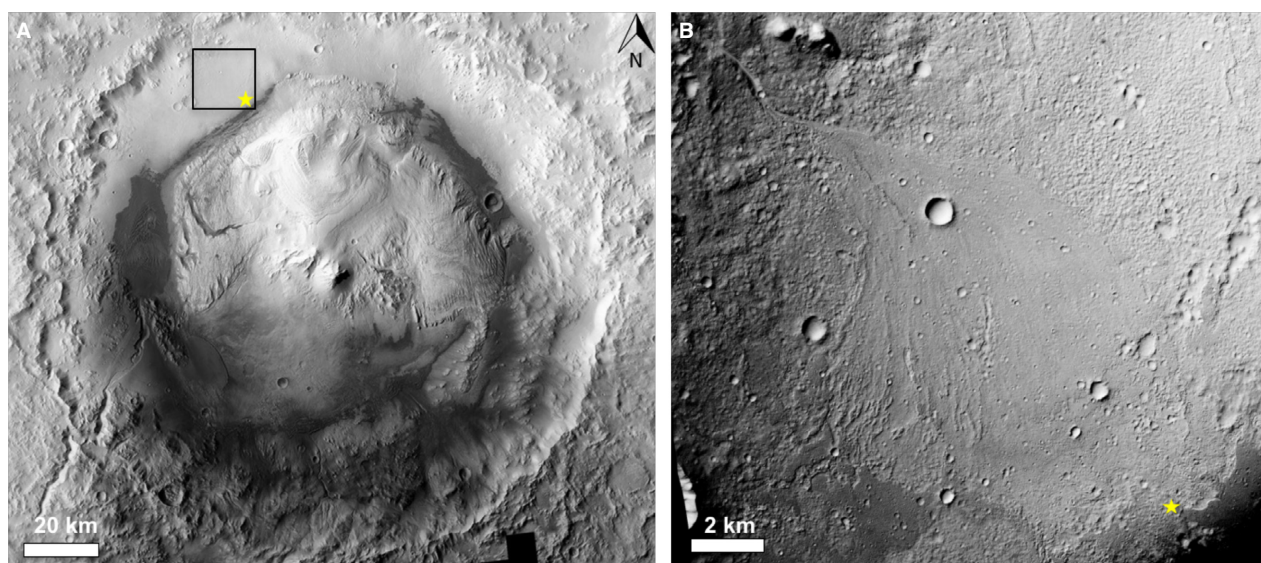**Fig. 1.** (A) Mars Reconnaissance Orbiter Context Camera (CTX) mosaic of Gale crater. Yellow star indicates the Mars Science Laboratory (MSL) landing site at Bradbury Landing. Black box indicates the location of (B). (B) The MSL landing site (yellow star) lies at the distal extent of the Peace Vallis fan. CTX image P22_009571_1756_XI_04S222W, north is up, illumination from upper left. Credit NASA/JPL/MSSS.
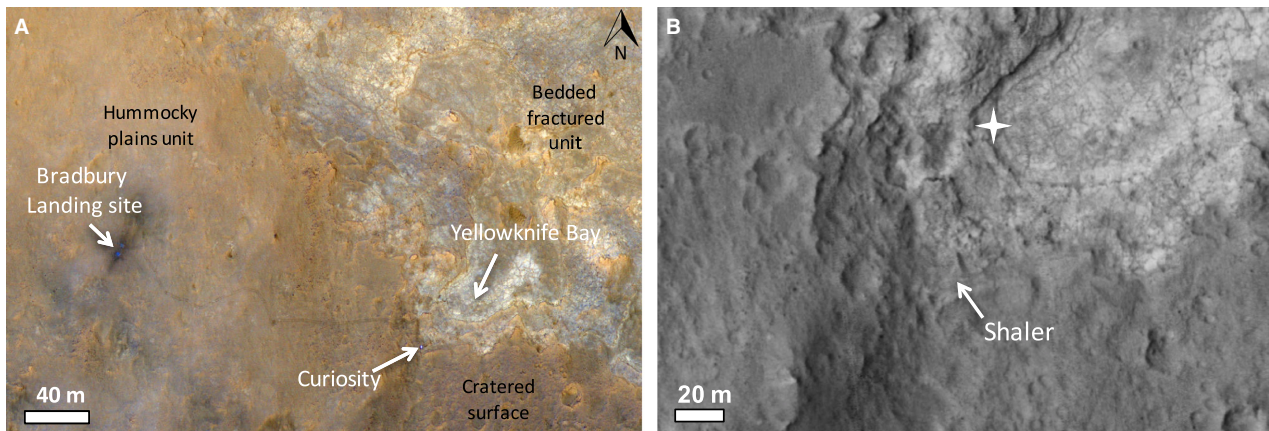
Fig. 2. (A) *Curiosity* traverse through the Glenelg area as of Sol 317, seen in HiRISE image ESP_032436_1755. The traverse is visible as dark, dust-free tracks leading from Bradbury Landing into Yellowknife Bay. Yellowknife Bay and the Shaler outcrop lie at the intersection of three orbital geological units: a hummocky plains unit, a bedded, fractured unit and a heavily cratered surface. *Curiosity* first drove past the Shaler outcrop on Sol 120 and revisited the outcrop during the egress from Yellowknife Bay. This image captures *Curiosity* during the investigation at the south-west portion of the Shaler outcrop. (B) Location of the Shaler outcrop on the margin of Yellowknife Bay. Cross indicates the location of the first drilling investigation in the Sheepbed mudstone, and the rover location for the context image in Fig. 3. Image credit: NASA/JPL/University of Arizona (illumination from left).

and the relatively smooth northern lowlands. Crater counts suggest that Gale crater formed at *ca* 3·6 Ga (Le Deit *et al.*, 2013, Thomson *et al.*, 2011) at the Noachian–Hesperian transition and that the crater-filling strata were deposited through the Early Hesperian time (Thomson *et al.*, 2011; Palucis *et al.*, 2014; Grant *et al.*, 2014; Grotzinger *et al.*, 2015). [Note that the Hesperian Period is defined from approximately 3·7 to 3·0 Ga and corresponds to the formation of extensive lava plains and occasional valley networks (Carr and Head, 2010). On Earth, this time period corresponds to the Archean.]

Incised valley networks are common in the region, suggestive of surface water flows (Cabrol *et al.*, 1999; Irwin *et al.*, 2005) towards the northern lowlands (DiBiase *et al.*, 2013). The *Curiosity* landing site at Bradbury Rise lies at the distal extent of a large ancient alluvial fan deposit, known as the Peace Vallis fan, which is sourced from the northern crater rim (Palucis *et al.*, 2014) (Fig. 1).

After landing at Bradbury Rise, *Curiosity* drove *ca* 400 m to the east to explore an area known as Glenelg, which represents the intersection of three distinct geological units as mapped from orbit (Grotzinger *et al.*, 2014; Vasavada *et al.*, 2014) (Fig. 2). These units were defined as a smooth hummocky unit ('HP'), a bedded, fractured unit ('BF') and a unit with a high density of preserved craters ('CS') (Grotzinger *et al.*, 2014). *Curiosity* performed a detailed investigation of

the stratigraphy exposed in Yellowknife Bay, which consists of the Sheepbed, Gillespie Lake and Glenelg members in ascending order (Fig. 3). This *ca* 5 m thick assemblage of sedimentary rocks is interpreted to represent a habitable fluvio-lacustrine environment (Grotzinger *et al.*, 2014). The lowermost Sheepbed member is a uniform grey smectite-containing mudstone (Vaniman *et al.*, 2014), interpreted as the result of settling from suspension in a lacustrine environment (Grotzinger *et al.*, 2014; Schieber *et al.*, 2017). The Gillespie Lake member is a poorly sorted, medium to very coarse-grained sandstone that is interpreted to have been deposited in unconfined flows on a distal fan lobe (Grotzinger *et al.*, 2014). The Glenelg member (*ca* 1·7 m thick) is inferred to be younger than the Sheepbed and Gillespie Lake members and contains a diverse suite of facies represented by the Point Lake, Shaler, Rocknest and Bathurst outcrops. Of these outcrops, Shaler was the first thick and laterally continuous exposure of cross-bedded sandstones documented by *Curiosity*.

METHODOLOGY

The Shaler investigation

Curiosity first observed the Shaler outcrop on sols 120 and 121 along the traverse into Yellowknife
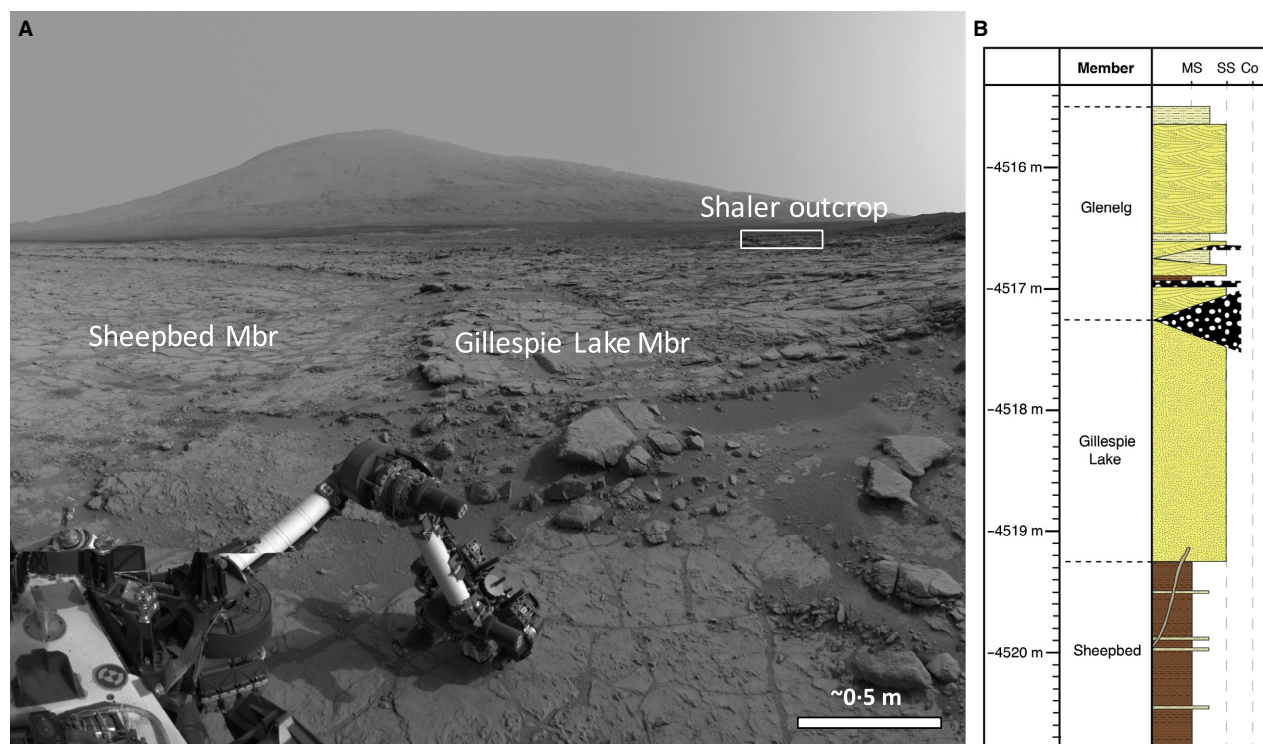
Fig. 3. (A) Stratigraphic context for the Shaler outcrop. The Shaler outcrop is part of the Glenelg member of the Yellowknife Bay formation, which lies stratigraphically above the Gillespie Lake sandstone and Sheepbed mudstone. View to the south, with Aeolis Mons in the distance. Navcam mosaic acquired on Sols 166 and 168 (ncam07754, ncam05794, ncam12754, ncam00365, ncam00350 and ncam00364). (B) Stratigraphic column modified from Grotzinger *et al.* (2014). The Glenelg member is represented by a diverse suite of facies and is generally coarser-grained than the underlying members. Grain sizes are denoted on the right-hand side of the column, including mudstone (MS), sandstone (SS) and conglomerate (Co).

Bay (Vasavada *et al.*, 2014). A more extensive investigation was carried out from sols 309 to 324, during which *Curiosity* carried out analyses at the north-eastern, middle and south-eastern portions of the outcrop. The stratigraphy, sedimentary structures and architecture of the Shaler outcrop are described as observed by the Mast Cameras (Mastcam), Navigation Cameras (Navcam), Mars Hand Lens Imager (MAHLI) and Chemistry Camera (ChemCam).

Instruments

Mastcam is a multispectral imaging system, which consists of two digital cameras mounted on the rover's mast (1·97 m above the ground). The left and right cameras have 34 mm (M34) and 100 mm (M100) focal lengths, yielding pixel scales of 0·22 and 0·074 mrad pixel^{-1}, respectively. Mastcam is capable of full colour panoramic and stereoscopic measurements (Malin *et al.*, 2010). Mastcam images were used to delineate

sedimentary structures, sedimentary facies, stratal bounding surfaces and sedimentary architecture, and determine dip directions of bedding.

Navcam consists of four digital cameras mounted on the rover's mast, attached to the same camera plate as the Mastcam and ChemCam instruments. For redundancy, there are two pairs of Navcams, but only one pair is active at a time. Navcam is capable of 360-degree panoramic imaging and provides stereo range data out to 100 m. Navcam has a 45-degree square field of view, and a pixel scale of 0·82 mrad pixel^{-1} (Maki *et al.*, 2012). Navcam images were used for targeting and to provide additional geological context.

The ChemCam instrument is also located on the rover's mast and consists of a laser-induced breakdown spectrometer (LIBS) and remote micro-imager (RMI) (Maurice *et al.*, 2012; Wiens *et al.*, 2012). The LIBS provides remote elemental compositions at distances of *ca* 2 to 7 m from the mast. The RMI provides high-resolution images to document the locations of the LIBS analyses, and can

Table 1. Summary of Mars Hand Lens Imager (MAHLI) targets at Shaler.

Sol	Target name	Image IDs	Working distance (cm)	Pixel scale (μm pixel^{-1})
322	Aillik	0322MH0001900010103948C00	26·5	100·3
		0322MH0001730010103950C00	6·8	30·9
		0322MH0001730010103960C00	6·8	30·9
		0322MH0003020010103970C00	3·8	20·2
		0322MH0002990010103980C00	6·9	31·3
		0322MH0002990010103990C00	7·0	31·4
		0322MH0002990010104000C00	6·8	30·7
		0322MH0002990010104010C00	7·0	31·7
323	Eqalulik	0323MH0001900010104078C00	26·6	100·5
		0323MH0001680010104080C00	7·0	31·4
		0323MH0001680010104090C00	6·9	31·3
		0323MH0003020010104100C00	4·0	20·9
324	Fleming	0324MH0003040010104148C00	30·8	115
		0324MH0003040010104150C00	32·1	120
323	Gudrid	0323MH0001900010104110C00	26·4	99·8
		0323MH0003030010104112C00	8·3	36·0
		0323MH0003030010104122C00	8·2	35·9
323	Howells	0323MH0001900010104044C00	26·6	100·5
		0323MH0001680010104046C00	6·9	31·0
		0323MH0001680010104056C00	6·8	31·0
		0323MH0003020010104066C00	3·8	20·3

also be used to identify grain sizes and sedimentary structures. The RMI has a field of view of 20 mrad and a pixel scale of 19·6 μm per pixel (Le Mouelic *et al.*, 2015). ChemCam acquired LIBS data and RMIs for a total of 28 non-soil targets at the Shaler outcrop (Anderson *et al.*, 2015).

The MAHLI is a high-resolution camera mounted on the rover's arm, capable of both colour and stereoscopic imaging. The MAHLI operates at working distances between 2·1 cm to infinity, with a maximum resolution of *ca* 14 μm pixel^{-1} (Edgett *et al.*, 2012); MAHLI images enable the identification of small-scale sedimentary structures and grain sizes. Five targets were selected for high-resolution imaging at the Shaler outcrop (Table 1). The MAHLI images used in this study were acquired at working distances between 3·8 cm and 32·1 cm, resulting in image scales ranging from 20 to 120 μm pixel^{-1}.

Data processing

Structural attitudes were obtained using Mastcam stereo data. Range and topographic data can be derived from Mastcam stereo image pairs. Linear segments along bedding planes were traced manually, and the corresponding topographic data were extracted. The natural curvature of the outcrop and of individual beds provided constraints on their three-dimensional geometry. A best-fit plane was calculated for each of the traced segments, and mathematical criteria ensured that the layers were well fit by a plane.

LARGE-SCALE STRATIGRAPHIC RELATIONS WITHIN SHALER OUTCROP

The Shaler outcrop is approximately 0·7 m thick and extends for more than 20 m in lateral extent for the main outcrop (Figs 4 and 5). A smaller outcrop of cross-stratified sandstones lies *ca* 3 to 4 m to the south-west (Fig. 6), but a small impact crater prohibits the direct correlation of these beds to the primary Shaler outcrop. Isolated exposures of stratified sandstones were also encountered prior to arrival at Yellowknife Bay (observed from the Rocknest outcrop, *ca* 40 m to the north-west of Shaler) (Edgar *et al.*, 2013), suggesting that the Shaler sandbody may have been more laterally extensive.

Shaler is distinguished from the underlying Gillespie sandstone member by the presence of well-developed, trough cross-stratification and bedsets that produce a platy weathering

Fig. 4. Overview of the Shaler outcrop. White lines illustrate the extent of the deposit (more than 20 m in lateral extent and *ca* 0·7 m thick). Boxes indicate the locations of following figures. Mastcam mosaics acquired on sols 110 to 113 (mcam00686 and mcam0096). Image credit: NASA/JPL-Caltech/MSSS.

character. The basal beds of Shaler appear to sharply overlie sandstones of the Gillespie Lake member. Local exposures reveal Shaler beds draping subtle topographic variations on the Gillespie sandstone surface (Fig. 5C and D).

The top of the Shaler outcrop is defined by a *ca* 10 cm thick resistant cross-stratified unit with a distinct geochemical signature (Anderson *et al.*, 2015) (Fig. 7). This resistant capping unit may be equivalent to a laterally extensive, erosionally resistant bed that preserves a higher density of craters on its upper surface. This surface may equate to the cratered surface (CS) defined by orbital mapping (Calef *et al.*, 2013; Grotzinger *et al.*, 2014; Jacob *et al.*, 2014). In the vicinity of the Shaler outcrop, there is not a clear overlying stratigraphic unit. After leaving Shaler, *Curiosity* climbed in elevation and encountered a number of cross-stratified sandstones and conglomerates along the traverse (Vasavada *et al.*, 2014). However, the stratigraphic relationship of these deposits to the Shaler outcrop is not constrained.

SEDIMENTARY FACIES

The Shaler outcrop of the Glenelg member comprises seven distinct sedimentary facies defined principally by grain size and sedimentary structures (Table 2; Fig. 8). In addition, erosional resistance to weathering of sedimentary beds, brightness and colour were used to help differentiate facies. Facies are presented in order of increasing grain size.

Facies 1: Fine-grained convolute-laminated facies

Description

This facies is characterized by convolute lamination in an approximately 5 cm thick bed (Fig. 9A). Individual laminae are *ca* 2 mm thick. Figure 9A shows a tight, isoclinal, recumbent fold. The fold hinge can be seen on the lower left side of the image, but it is difficult to observe the geometry on the right side because the block is broken. Individual laminae also show evidence for minor buckling. The deformed interval is exposed for 0·5 m, and only one fold is visible. This facies was not captured in MAHLI or Chem-Cam RMI images, so detailed grain-size data are not available. It appears to comprise grain sizes finer than the Mastcam M100 can resolve (Fig. 9A), which at this distance is approximately 300 micrometres (*μ*m), suggesting that the grain
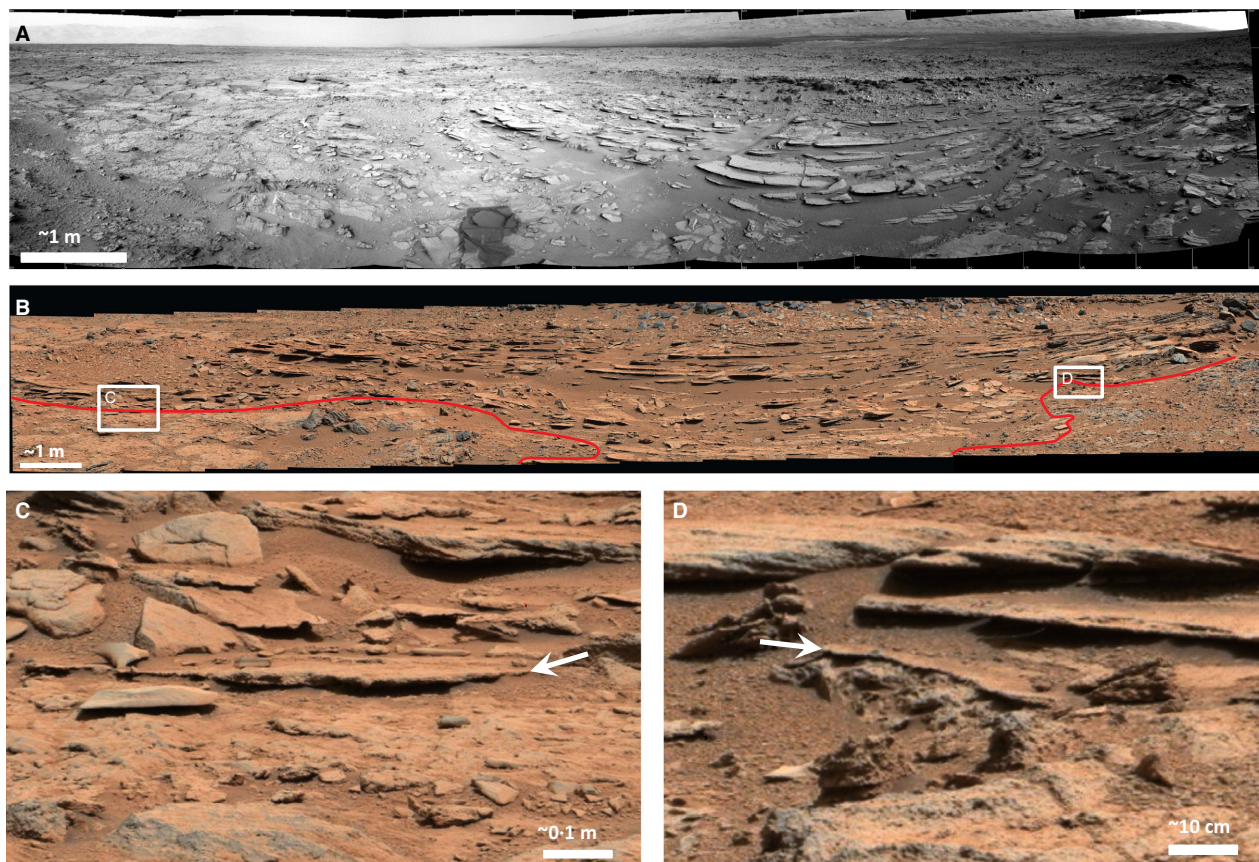
Fig. 5. (A) The full extent of the Shaler outcrop is seen in this Navcam mosaic acquired on Sol 120 (ncam00213 and ncam00215). The top of the outcrop is defined by a resistant unit which may equate to the laterally extensive cratered surface (CS) defined by orbital mapping. (B) Shaler infills three shallow palaeodepressions in the Gillespie sandstone surface, marked by the red line. Mastcam mosaic acquired by the M100 camera on Sol 120, mcam00752. White boxes indicate the locations of (C) and (D). (C) and (D) The contact with the underlying Gillespie sandstone is clearly observed at the north-east and south-west ends of the outcrop. Shaler beds drape palaeotopography on the upper surface of the Gillespie sandstone. Image credit: NASA/JPL-Caltech/MSSS.

size of this facies is finer than medium sand. This facies is only observed just above the contact between the Gillespie and Shaler units at the north-eastern end of the outcrop.

Interpretation
This facies is interpreted to represent soft-sediment, plastic deformation of partially liquefied sediment shortly after deposition. The convoluted bed may be the result of dewatering in response to sediment loading, or in response to sediment movement on a slope. Liquefaction is a common process in unconsolidated sediment of fine to medium sand size (Owen & Moretti, 2011; Owen *et al.*, 2011) and is abundant in pre-vegetation fluvial systems on Earth (Owen & Santos, 2014).

Facies 2: Fine-grained, evenly horizontally laminated sandstone

Description
Facies 2 comprises fine-grained sandstone characterized by sub-horizontal, highly parallel and regular millimetre-scale laminae (Fig. 9B). The laminae appear to be sharp-based and have a 'pinstripe' character. No cross-lamination is evident. This facies was not captured in MAHLI or ChemCam RMI images, so detailed grain-size data are not available. However, the grains are smaller than the Mastcam M100 can resolve (Fig. 9B), which at this distance is approximately 516 microns, suggesting that the grain size of this facies is medium sand or finer. This facies occurs as minor bedsets locally in the outcrop, although it is predominantly observed at the north-eastern end.
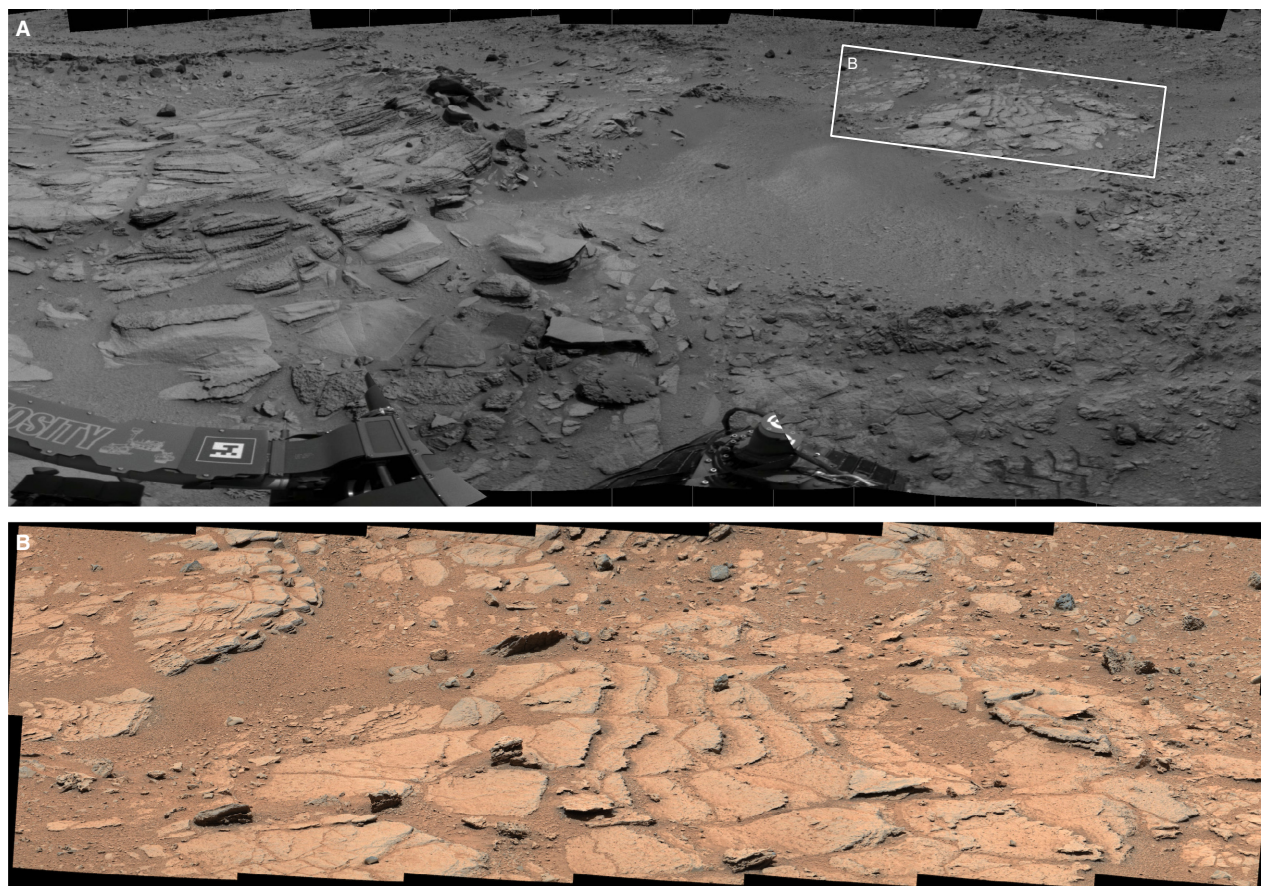
Fig. 6. (A) Navcam orthomosaic acquired on Sol 317 showing an outcrop of cross-stratified sandstones separated from the main Shaler outcrop by a small impact crater. Navcam mosaic N_L000_0317_ILT006CYL_S_0804_UN-CORM1. (B) Mastcam mosaic acquired on Sol 319 illustrating that the small outcrop is similar to the main Shaler sandbody, suggesting that the Shaler outcrop may have been more laterally extensive. Mastcam sequence mcam01307. Image credit: NASA/JPL-Caltech/MSSS.

Interpretation

The highly parallel geometry of the laminations and their pinstripe character lead to the interpretation that this facies records the deposits of subcritically climbing translatent wind ripples (Hunter, 1977a,b; Fryberger & Schenk, 1988) which suggests aeolian reworking of fluvially transported sands. Alternatively, this facies could be interpreted as suspension fallout lacustrine deposits, or upper flow regime planar bedding. Due to the limited data available, and the isolated occurrences of this facies, the distinction between planar-bedded aeolian deposits and lacustrine or upper flow regime deposits cannot be made.

Facies 3: Light-toned cross-stratified sandstone

Description

This facies is found in the lower part of the south-western end of the outcrop. This facies is characterized by fine, millimetre-scale, trough cross-lamination in decimetre-scale bedsets (Fig. 9C). Grain-size analyses using ChemCam RMIs indicate that the largest grains are medium to coarse sand; however, most grains are unresolvable over the visible RMI area (Anderson *et al.*, 2015) (Fig. 10A). The MAHLI images of the target Aillik provide additional grain-size information, indicating that the majority of this facies is fine-grained and well-sorted (Fig. 11A and B), with observable grain sizes ranging from 100 to 150 μm. However, this facies is very well-cemented, which makes it difficult to identify individual grains over much of the exposed area. Facies 3 is captured in ChemCam targets named Aillik, Menihek and Fabricius Cliffs, and the MAHLI target Aillik (Fig. 10A and B).

Interpretation

This facies is interpreted to represent the migration of dune-scale bedforms. The finer average
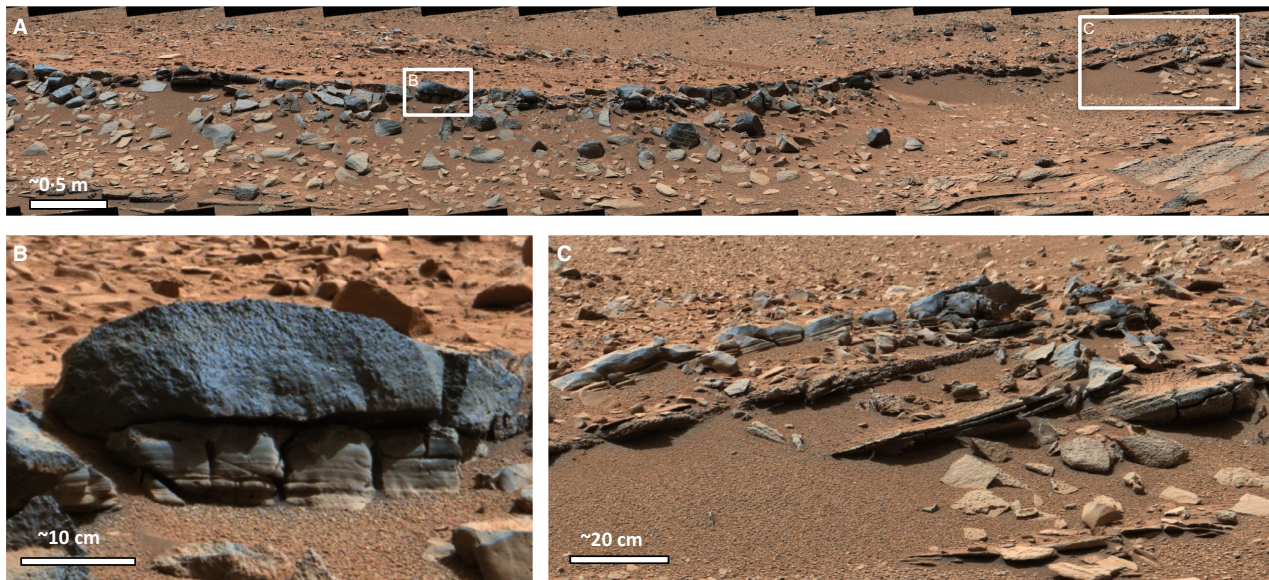
Fig. 7. (A) The uppermost part of the outcrop is formed by a resistant unit. Mastcam mosaic acquired by the M100 camera on Sol 319; mcam01305. White boxes indicate the locations of (B) and (C). (B) The uppermost part of the outcrop is comprised of coarse-grained cross-stratified sandstone facies, and fine-grained well-laminated facies. Image M100 was acquired from a slightly different viewing geometry on Sol 319, mcam01293. (C) At the south-west end of the outcrop, discrete lenses of resistant coarse-grained sandstones are visible, interbedded with less-resistant, presumably finer-grained packages. Image credit: NASA/JPL-Caltech/MSSS.

Table 2. Shaler sedimentary facies.

Facies	Description	Interpretation
1	Fine-grained convoluted facies	Soft-sediment deformation soon after deposition
2	Fine-grained evenly laminated sandstone facies	Aeolian wind-ripple stratification, reworking of fluvial sands
3	Light-toned cross-stratified fine-grained sandstones	Straight and sinuous crested bedforms of finer average grain size
4	Recessive weathering, laminated sandstone facies with vertical fractures	Desiccation cracks, indicative of intermittent wetting and drying
5	Single set, cross-stratified pebbly sandstones	Straight and sinuous crested bedforms
6	Stacked planar and trough cross-stratified pebbly sandstones	Sinuous crested bedforms superimposed on a bar or fan surface
7	Smooth cross-stratified facies, composed of two subfacies: (i) coarse-grained cross-stratified facies; (ii) fine-grained well-laminated facies, with occasional nodules	A new dispersal system, different sediment provenance. The coarse-grained cross-stratified subfacies represents dune migrations, while the fine-grained well-laminated subfacies may represent upper plane bed and/or fallout from suspension.

grain size of this lens represents a different sediment calibre than the surrounding deposits, suggesting local variation in grain-size supply and flow conditions within the system. Given the available data, a subaqueous or subaerial origin cannot be distinguished.

Facies 4: Recessive weathering, laminated facies with vertical fractures

Description
This facies occurs at the top of small-scale fining-upward successions that are present at
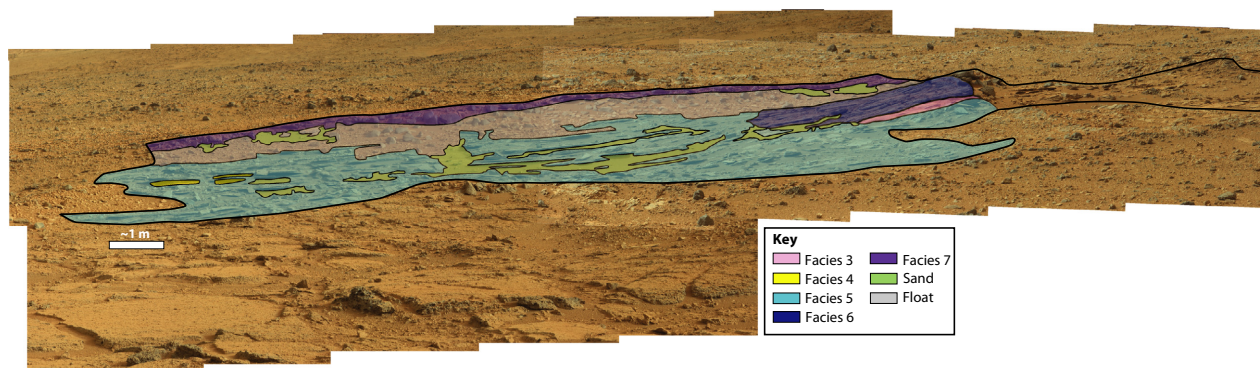
Fig. 8. Facies map showing the distribution of Facies 3 to 7. Facies 1 and 2 are not visible from this perspective, but are located in the lower north-east portion of the outcrop (the lower left region in this mosaic). View is towards the east. Facies are not mapped in the far south-west portion of the outcrop (right side of the mosaic) because the rover did not investigate this region in detail, but the outcrop is outlined. Mastcam mosaics acquired on sols 110 to 113 during initial drive by of the Shaler outcrop (mcam00686 and mcam0096). Image credit: NASA/JPL-Caltech/MSSS.

the north-eastern end of the outcrop (Figs 9D and 10B). The most distinctive feature of this facies is the local presence of vertical fractures that originate from the same bed and extend through several beds (Fig. 9D). The linear fractures are approximately 1 cm wide and up to 15 cm long. The fractures are more resistant than the beds they disrupt. Across Aeolis Palus, this facies has only been observed in the Shaler outcrop, but may be difficult to identify elsewhere because of its recessive and friable nature, which may result in poor preservation. Whereas grain-size data are not available for the fractures, their roughness and resistance as observed in Mastcam images suggest that they are infilled with sand. This facies was recorded in the ChemCam observations of targets named Rove and Rusty Shale; however, the fracture fills were not captured by ChemCam.

Interpretation
This facies is interpreted to be relatively finer-grained because of its recessive weathering character and may represent fallout from suspension in a subaqueous environment. The present authors interpret the vertical fractures as desiccation cracks that are indicative of intermittent wetting and drying. An alternative explanation is that the vertical fractures are diagenetic features, such as veins or sand injectites, although their limited occurrence and abrupt termination at the same bed favour the former interpretation.

Facies 5: Single set, cross-stratified pebbly sandstones and sandstones

Description
This facies forms the majority of the outcrop and is expressed as centimetre-thick, well-cemented beds, commonly but not always separated by recessive gaps (Fig. 9E). This facies appears brighter than surrounding facies, and measureable grain sizes range from coarse sand to fine gravel, up to 3 mm in diameter (Anderson *et al.*, 2015) (Fig. 10C). The coarsest grains line the base of bedsets, and bedsets are typically 5 to 10 cm thick. The facies is characterized by trough cross-bedding. Troughs are up to 1 m wide, and foresets are typically concave up and tangential. Locally rib and furrow structures are preserved on bedding planes, which clearly indicate trough orientations (see *Palaeocurrent analysis* section). Small superimposed ripple cross-stratification is also observed. Bedsets of ripple cross-stratification are *ca* 1 to 3 cm thick. Where climbing bedforms are visible, they climb at subcritical angles, resulting in preservation of only the lee slope deposits. Facies 5 is recorded in a number of ChemCam targets, including Stanbridge, Port Radium, Ramah, Michigamme, Wakham Bay, Piling, Wishart, Gogebic, Saglek, Montaigne, Double Mer, Camp Island and Seal Lake.

Interpretation
This facies is interpreted to represent deposition from the migration of subaqueous bedforms. The
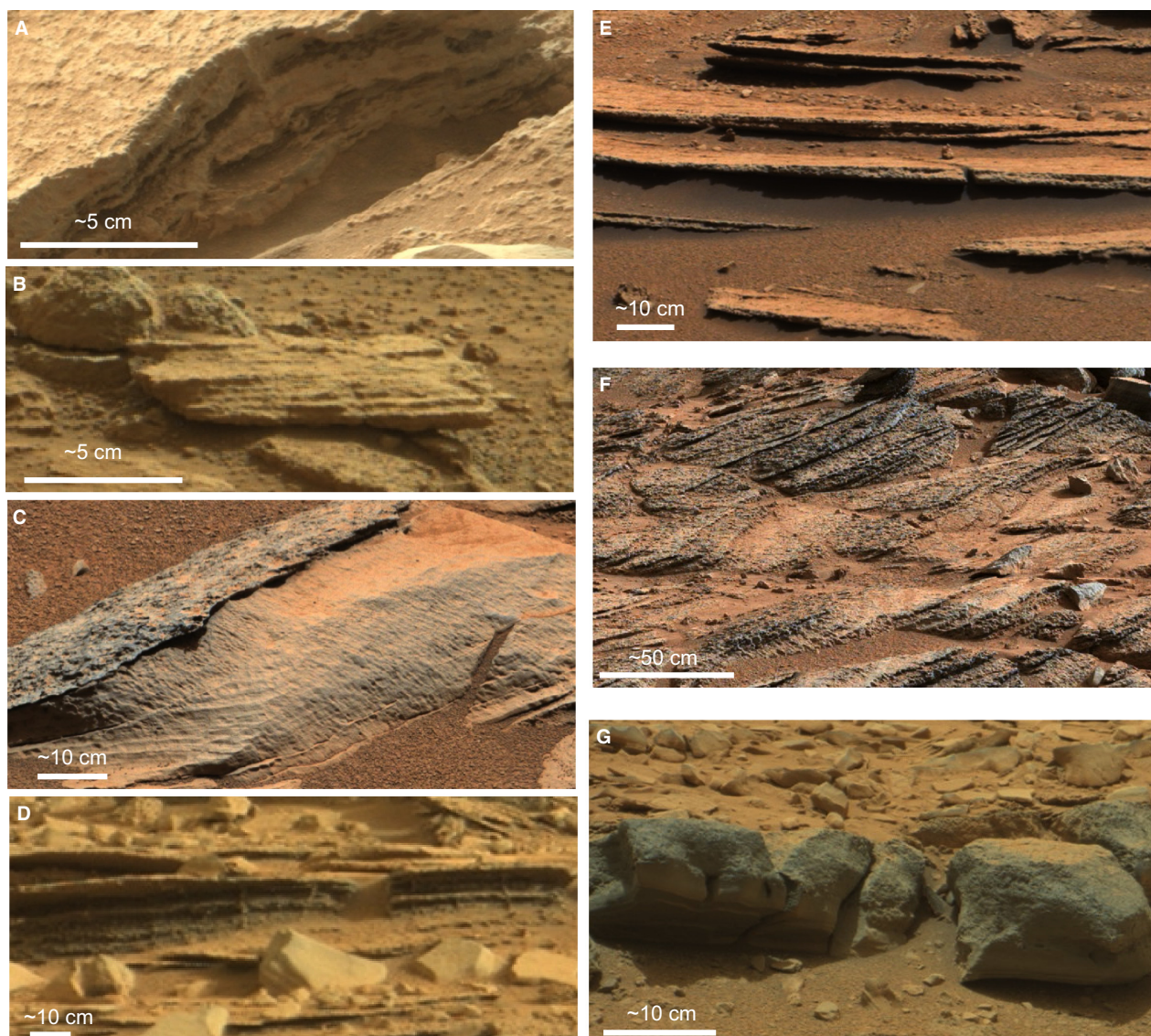
Fig. 9. Sedimentary facies identified at the Shaler outcrop. See text for full descriptions. (A) Facies 1: Fine-grained convolute-laminated facies (Mastcam mosaic acquired on Sol 311, mcam01279). (B) Facies 2: Fine-grained, evenly horizontally laminated sandstone (Mastcam mosaic acquired on Sol 311, mcam01279). (C) Facies 3: Light-toned cross-stratified sandstone (Mastcam mosaic acquired on Sol 121, mcam00756). (D) Facies 4: Recessive weathering, laminated facies with vertical fractures (Mastcam mosaic acquired on Sol 113, mcam00696). (E) Facies 5: Single set, cross-stratified pebbly sandstones and sandstones (Mastcam mosaic acquired on Sol 120, mcam00752). (F) Facies 6: Stacked planar and trough cross-stratified pebbly sandstones (Mastcam mosaic acquired on Sol 120, mcam00753). (G) Facies 7: Blue grey, smooth-weathering cross-stratified sandstone (Mastcam mosaic acquired on Sol 309, mcam01275). Image credit: NASA/JPL-Caltech/MSSS.

trough cross-bedding indicates deposition by migration of trains of three-dimensional sinuous crested sand dunes (Rubin & Carter, 2006). The observed fine gravel is coarser and more poorly sorted than is typical of wind transport, making aeolian deposition less likely, and thus this facies is interpreted as the result of bedload fluvial transport and deposition.

Facies 6: Stacked planar and trough cross-stratified pebbly sandstones

Description
This facies is found at the south-western end of the outcrop and is defined by compound cross-stratification (Figs 9F and 13D). It has a darker appearance than surrounding facies, and
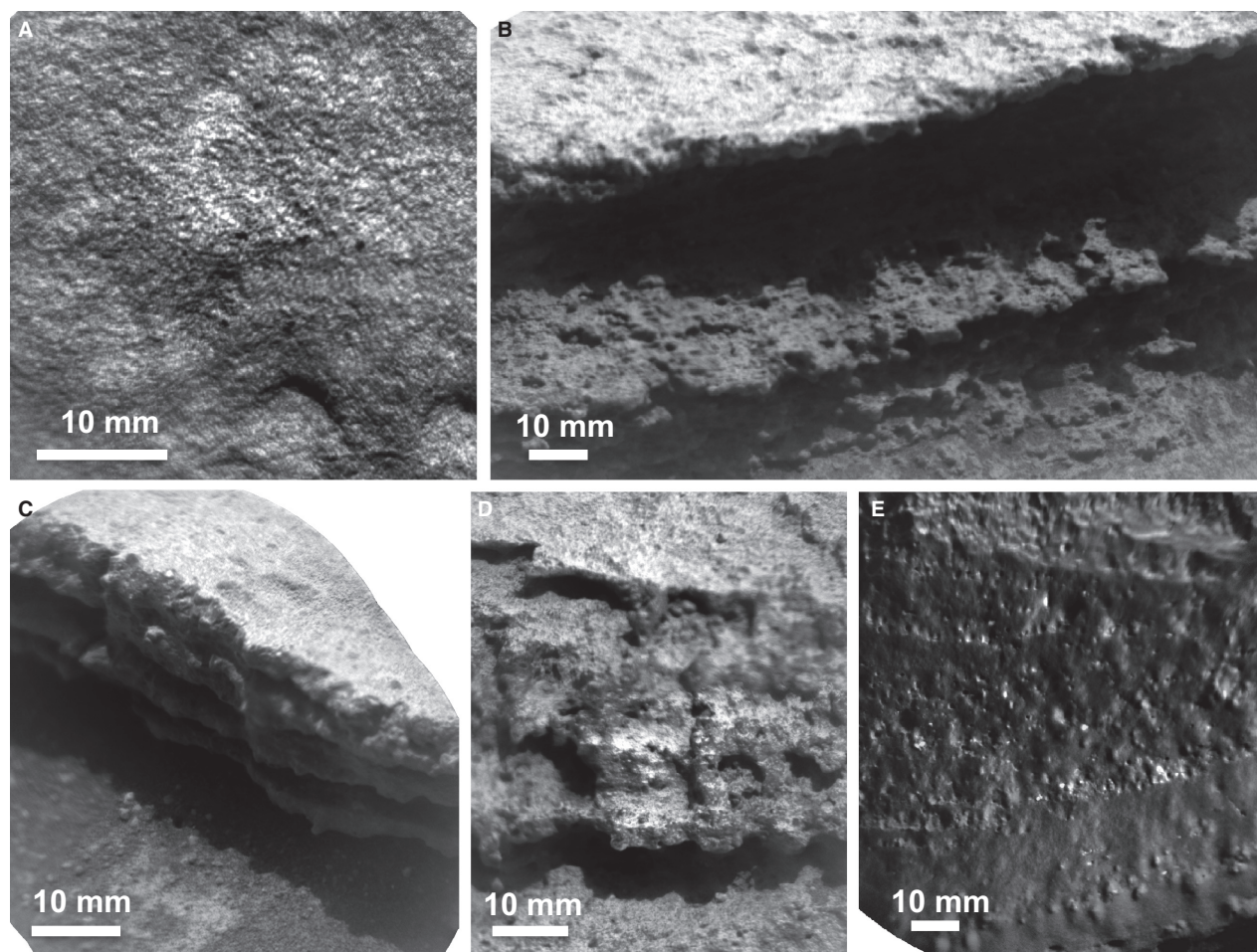
Fig. 10. Grain size and stratification revealed in ChemCam RMI images. (A) Target Aillik (Facies 3), acquired on Sol 319, ChemCam sequence ccam01319. (B) Target Rusty Shale (Facies 4), acquired on Sol 316, ChemCam sequence ccam01316. (C) Target Double Mer (Facies 5), acquired on Sol 317, ChemCam sequence ccam02317. (D) Target Cartwright (Facies 6), acquired on Sol 319, ChemCam sequence ccam04319. (E) Target Mary River (Facies 7), acquired on Sol 316, ChemCam sequence ccam04316.

a distinctive pitted weathering texture. Chem-Cam RMI images indicate that this facies is poorly sorted, and contains grains up to coarse sand and pebble (Fig. 10D) (Anderson *et al.*, 2015). The MAHLI images of the targets Eqalu-lik and Howells reveal subrounded granules and pebbles within the sandstones (Fig. 11C to H), some of which show collision marks (Fig. 11H). Pebbles up to 0·5 cm across are observed. Individual beds range from several millimetres thick to 1 cm thick. Bedsets are typically *ca* 5 to 10 cm thick (Fig. 9F). Troughs up to 0·5 m wide are visible in places (Fig. 13D). Facies 6 is captured in ChemCam targets Eqalulik, Cartwright, Steep Rock and Howells, as well as MAHLI targets Eqalulik and Howells.

Interpretation

This facies is interpreted to represent the migration of unidirectional subaqueous bedforms. Trough cross-bedding indicates that the majority of the bedforms had sinuous crestlines. Grain sizes of fine gravel are too coarse to be transported by the wind, ruling out aeolian deposition. The presence of compound cross-stratification indicates that the bedforms were superimposed on a larger-scale accretionary macroform such as a barform.

Facies 7: Blue grey, smooth-weathering cross-stratified sandstone

Description

Facies 7 forms a distinct unit at the uppermost part of the Shaler outcrop, providing a resistant

Fig. 11. Grain size and stratification revealed in MAHLI images. Four examples are presented, with image pairs illustrating MAHLI context and close-up views of the same target (credit: NASA/JPL/MSSS). (A) Target Aillik, a bright cross-stratified sandstone (Facies 3). MAHLI image acquired on Sol 322 at a working distance of 26·5 cm, 0322MH0001900010103948C00. (B) Well-sorted medium-sized sand grains and faint lamination are visible at Aillik. MAHLI image acquired at a working distance of 3·8 cm, 0322MH00030200101 03970C00. (C) Target Fleming, a pebbly sandstone (Facies 6). MAHLI image acquired on Sol 324 at a working distance of 30·8 cm, 0324MH0003040010104148C00. (D) Close-up of the same image of Fleming, showing coarse sand and granules. (E) Target Howells, another example of pebbly sandstone (Facies 6). MAHLI image acquired on Sol 323 at a working distance of 26·6 cm, 0323MH0001900010104044C00. (F) Coarse-grained sand and pebbles are visible at Howells, despite the pitted surface texture. MAHLI image acquired at a working distance of 3·8 cm, 0323MH0003020 010104066C00. (G) Target Gudrid, a pebbly sandstone (Facies 6). MAHLI image acquired on Sol 323 at a working distance of 8·2 cm, 0323MH0001900010104110C00. (H) Close-up of the same image of Gudrid, showing a subrounded grain with collision marks (arrow), typical of bedload transport.
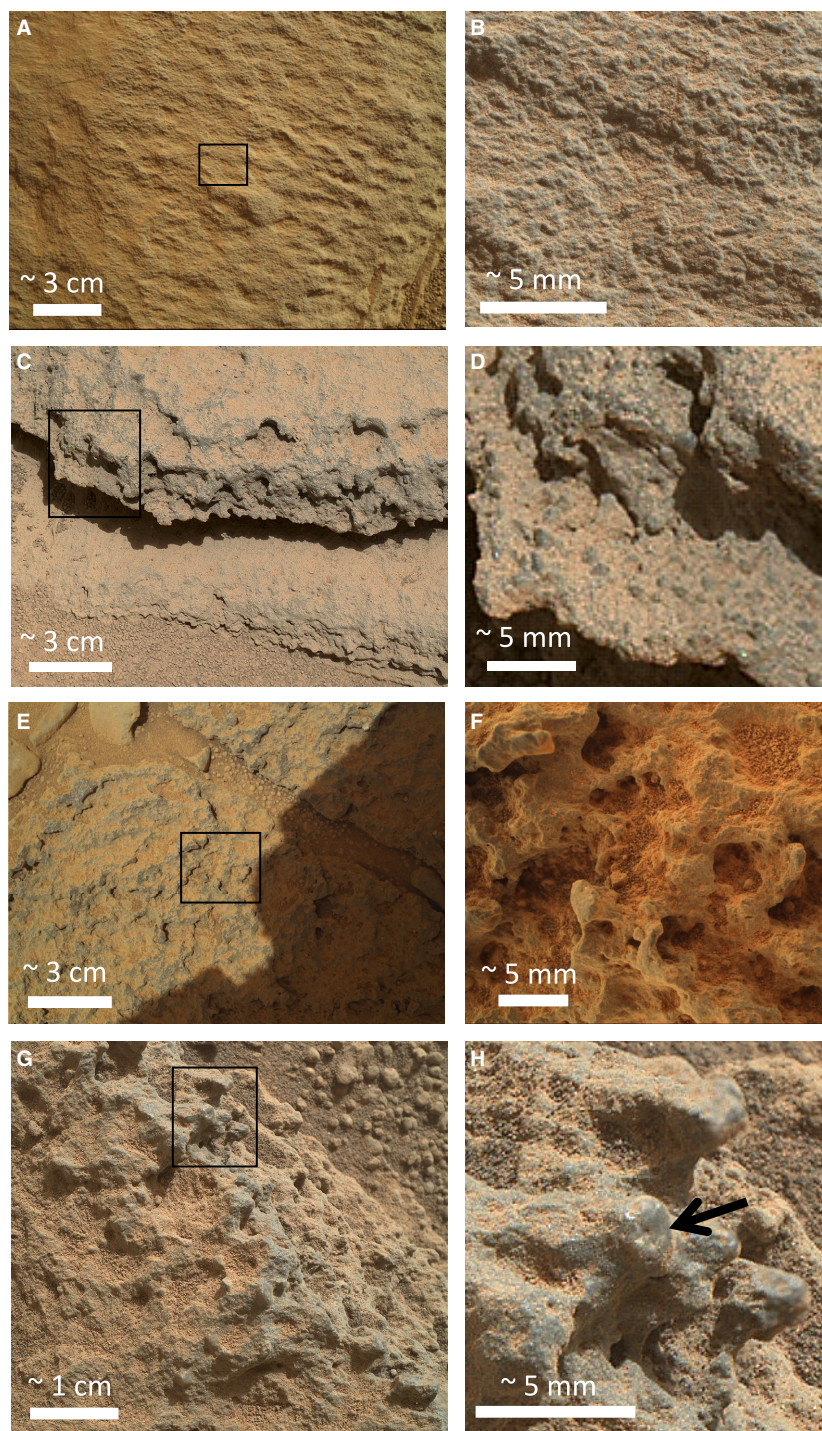
cap at the top of the outcrop, which may equate to a more extensive cratered surface. It is characterized by a darker tone than the rest of the Shaler outcrop and shows a distinct blue grey colour in Mastcam images (Fig. 9G). Rock faces for this facies show a smoother weathering appearance than the underlying Shaler facies. Facies 7 can be divided into two subfacies with distinct grain sizes (Fig. 7B). Facies 7A consists of coarse-grained cross-stratified sandstones up to 10 cm thick; Facies 7B consists of fine-grained planar-laminated sandstones with occasional nodules, exposed in beds up to 5 cm thick. Facies 7A is represented by ChemCam targets named Mary

River, Chioak and Husky Creek. Based on Chem-Cam RMIs, the coarser-grained component appears to be well-sorted and contains grains up to granule size (Fig. 10E) (Anderson *et al.*, 2015). The finer-grained component is well-laminated and composed of grains finer than Mastcam can resolve (Fig. 7B), which at this distance is about 1 mm.

Interpretation

The coarse-grained cross-stratified subfacies represents deposition from migrating fluvial dunes, whereas the fine-grained well-laminated subfacies may represent upper plane bed deposition or fallout from suspension. Fluctuations between subfacies record variation in flow conditions. The darker colour than the lower Shaler outcrop is interpreted as the result of the absence of dust on many faces, possibly due to its resistant cliff-forming nature, but the colour difference could be intrinsic.

Palaeocurrent analysis

The Shaler outcrop is characterized by well-developed, large-scale trough cross-bedding, and the presence of several outcrop-length surfaces that dip *ca* 10 to 15° towards the south-east quadrant. These outcrop-length surfaces are interpreted as bounding surfaces, which define sets of subaqueous dunes. Dip azimuths of the outcrop-length surfaces vary across the outcrop from approximately east at the south-west edge to approximately south-east at the north-east edge (Fig. 12). In planform (map view), these surfaces record a subtle south-east-facing concavity on which the south-east-dipping beds were deposited. The dip of these outcrop-length surfaces is interpreted to be primary rather than the result of post-depositional tilt. The beds that are bounded by the outcrop-length surfaces, which are low-angle to angle-of-repose, and the underlying Gillespie sandstone is flat-lying, which would be difficult to preserve if the outcrop had undergone significant deformation.

While this large-scale feature with a south-east-facing concavity advanced towards the south-east, superimposed bedforms migrated across its surface and deposited small trough-shaped sets of cross-bedding, represented by Facies 5 and 6 (Fig. 13). Foresets within these sets have a wide range of dip azimuths, consistent with trough cross-bedding. However, the fortuitous preservation of troughs in three dimensions, and in particular the planform preserved on bedding surfaces (Fig. 13C), permits accurate determination of the long axes of troughs. Axes of trough cross-sets have been noted to be generally aligned parallel to local flow direction and show a relatively small degree of scatter (Dott, 1973; Michelson & Dott, 1973; High & Picard, 1974). The long axis orientations of troughs indicate migration of bedforms to the north-east. An exception to the dominant north-east transport direction is the lowermost part of the outcrop. The base of the section appears to infill subtle topographic variations in the Gillespie sandstone surface, and cross-stratification in the lower outcrop records a wider range of transport directions. This diversity may record local variability in the flow due to topographic effects.

Small sets of cross-laminae (*ca* 3 cm thick) deposited by superimposed ripples are also present (Fig. 13B). Ripple foresets suggest a dominantly south-westward migration direction, opposite to that of the large-scale dunes. These ripples are interpreted as back-flow ripples, formed in lee-side eddies (Herbert *et al.*, 2015). The presence of back-flow ripples provides additional information about the flow conditions. It has been suggested that back-flow ripples form in association with constructive dunes under conditions when relatively fine sediment is deposited in the lee-side eddy (Martinius & Van den Berg, 2011). The presence of multiple orders of bedforms within each sediment package indicates short episodes of sustained surface flow, although the sustained flow may not have lasted more than hours to days.

SEDIMENTARY ARCHITECTURE

Mastcam mosaics obtained from multiple viewing geometries enable high-resolution characterization of the sedimentary architecture of the Shaler outcrop. These data reveal marked variation in grain size, bedding geometry and stratification style within the outcrop. Genetically related sedimentary bedsets that record distinct stages in the depositional evolution at the Shaler outcrop are described below. The Shaler outcrop can be subdivided into three units: Unit 1 is defined by bedsets that infill three palaeo-depressions at the base of the section; Unit 2 forms the laterally continuous bulk of the section; and Unit 3 represents the resistant uppermost bedsets of the outcrop marked by a change in texture and chemistry (Fig. 14).
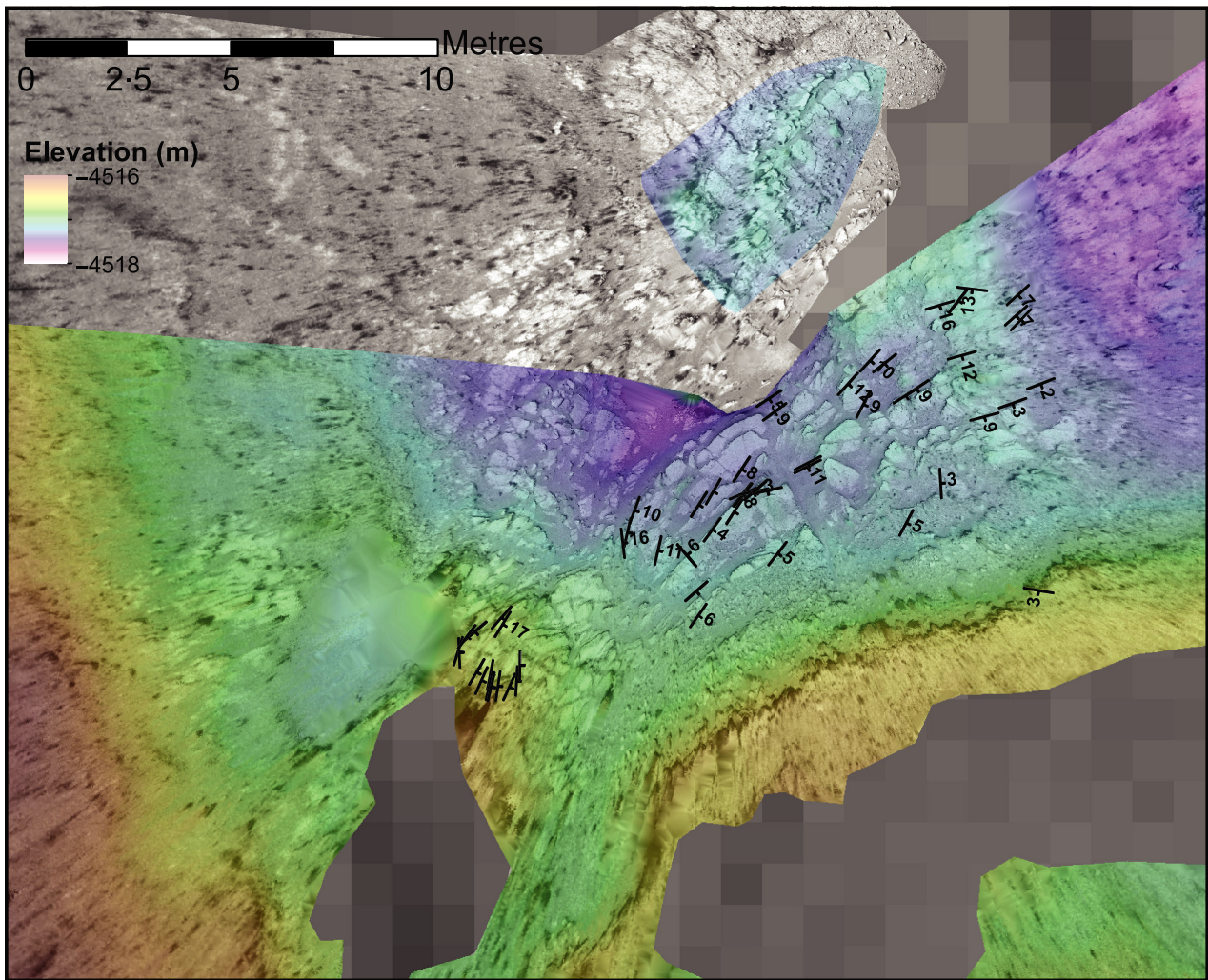
Fig. 12. Strike and dip measurements acquired for large-scale surfaces (within facies 5 and 6) across the Shaler outcrop (north is up). Surfaces dip approximately 10 to 15 degrees to the south-east. Measurements are plotted on a Navcam orthomosaic to show the complete outcrop. Measurements were acquired from Mastcam stereo mosaics acquired on sols 309, 311, 315, 316 and 319 (sequence IDs mcam01275, mcam01279, mcam01292, mcam01298, mcam01305, mcam01306 and mcam01307).

Unit 1

Unit 1 records the infilling of subtle topographic variations on the Gillespie Lake sandstone surface. The lower part of the Shaler outcrop reveals three distinct sections that are *ca* 5 to 10 m wide (Fig. 14). Each section is infilled by a distinct assemblage of sedimentary facies. All three sections are dominated by cross-stratified sandstones of Facies 5 and 6 indicating dominantly fluvial deposition (cf. Fig. 13). The north-east section is characterized by thin resistant beds separated by recessive intervals and comprises Facies 1, 2, 4 and 5 (fine-grained convoluted facies, fine-grained evenly laminated sandstone facies, recessive weathering laminated sandstone facies with vertical fractures, and single set cross-stratified pebbly sandstones). The possible presence of aeolian wind-ripple-laminated strata and potential desiccation cracks suggests that fluvial deposition in this section was intermittent.

The central section of Unit 1 is *ca* 5·5 m wide. It is dominated by trough cross-stratified sandstones of Facies 5 (single set, cross-stratified pebbly sandstones) (Fig. 13A to C). These sandstones show marked variability in flow direction as interpreted from foreset dip directions of cross-stratified units. In general, trough cross-bedding suggests flow towards the easterly hemisphere; this suggests that fluvial flows infilled the depression locally from the west.
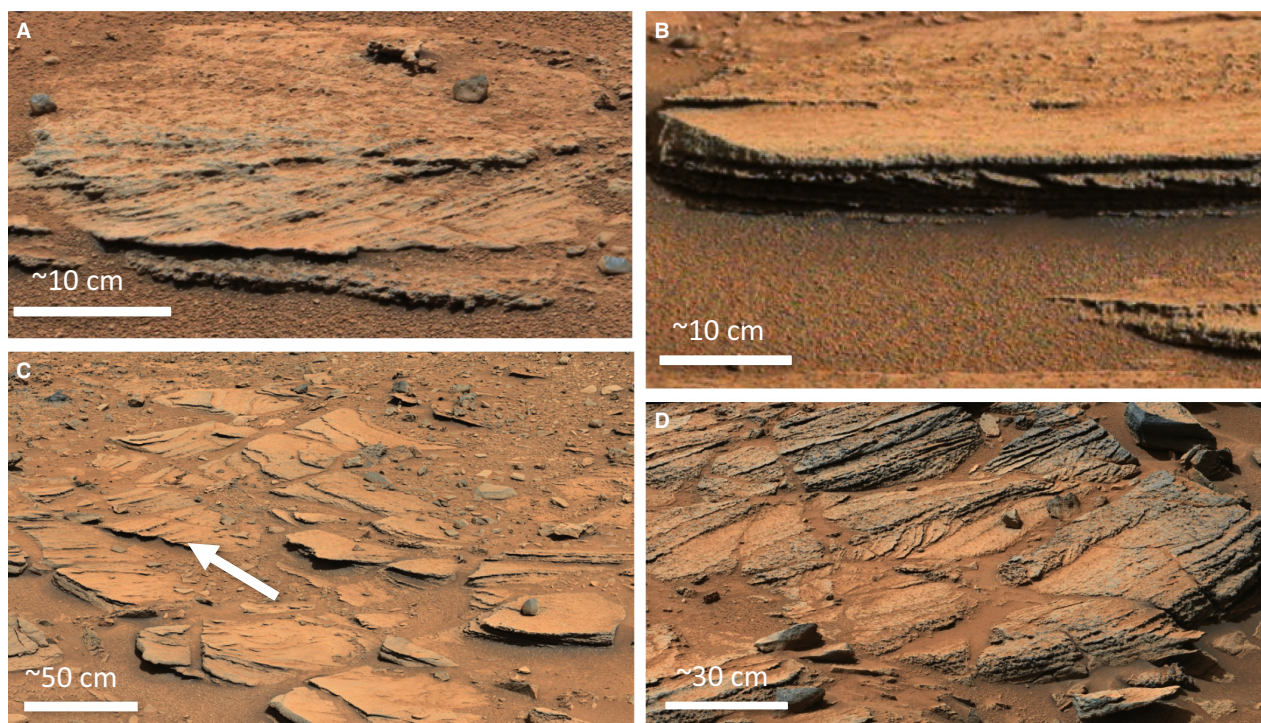
Fig. 13. Examples of cross-stratification within the Shaler outcrop. (A) Simple cross-stratification, indicating bedform migration from right to left (towards the north-east). Note the gravel base, fining upward into cross-stratified sandstone. Mastcam mosaic acquired on Sol 318 by the M100 camera, mcam01302. (B) Close-up of small ripple cross-stratification indicating migration from left to right, superimposed on larger-scale trough cross-bedding (larger-scale cross-bedding is not visible at this scale). Mastcam mosaic acquired on Sol 120 by the M34 camera, mcam00753. (C) Decimetre-scale trough cross-stratification. View looks down the axis of a trough (white arrow) and indicates bedform migration towards the north-east. Mastcam mosaic acquired on Sol 315 by the M100 camera, mcam01291. (D) Compound cross-stratification observed at the south-west end of the outcrop. Trough cross-bedding indicates that the dunes that deposited these sets had sinuous crestlines and migrated primarily towards the north-east. Set boundaries dip to the south-east, suggesting that the bedforms were superimposed on a larger-scale bar or fan surface. Mastcam mosaic acquired on Sol 319 by the M100 camera, mcam01306. Image credit: NASA/JPL-Caltech/MSSS.

The south-western end of the Shaler outcrop provides the most well-exposed stratigraphy (Fig. 15). Here, the top of the south-western section is contiguous with the upper part of the central section. At its base, beds can be observed to drape the Gillespie Lake erosional surface (Fig. 5C and D). The south-western section of Unit 1 is dominated by coarser-grained pebbly sandstones with one distinct lens of fine-grained cross-stratified sandstone (target Aillik, Facies 3) (Fig. 9C). The pebbly sandstones at the base of Unit 1 show more variability in transport direction than the rest of the Shaler outcrop.

Interpretation
Unit 1 records the initiation of Shaler fluvial deposition on top of the sandstones of the Gillespie Lake member. While the present surface topography does not reveal much vertical relief in Unit 1, the distinct facies and lack of bed continuity between the north-east, middle and south-east sections indicate that these parts of the outcrop were once separated, probably due to subtle topographic variations on the Gillespie sandstone surface. Based on these observations, the presence of three palaeo-depressions is inferred.

Unit 2

Unit 2 is defined as the continuous part of the Shaler sandbody. It extends across the entire length of the main outcrop (*ca* 20 m) (Fig. 14). Mastcam mosaics from multiple viewing geometries enable the identification of several outcrop-length surfaces, which can be used to correlate different bedsets across the outcrop (Fig. 16).
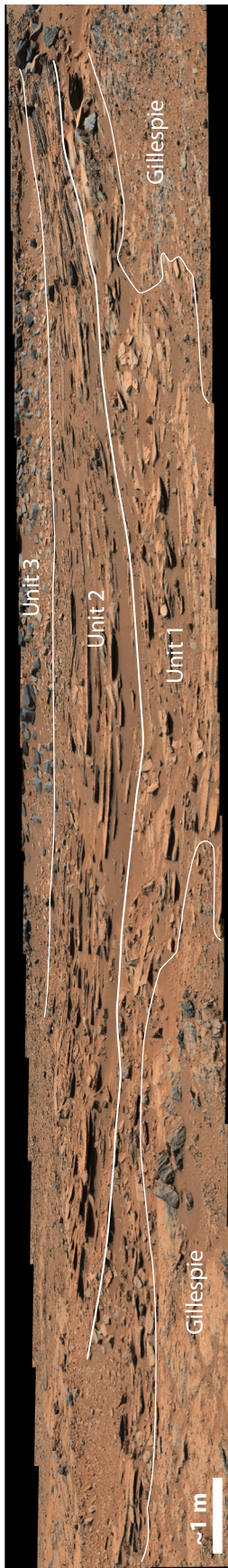
Fig. 14. The three distinct units observed within the Shaler outcrop, as seen in Mastcam M100 mosaic mcam00752, acquired on Sol 120. Unit 1 is defined by bedsets that infill three palaeo-depressions at the base of the section, Unit 2 forms the laterally continuous bulk of the Shaler outcrop, and Unit 3 represents the more resistant uppermost bedsets of the outcrop. Image credit: NASA/JPL-Caltech/MSSS.
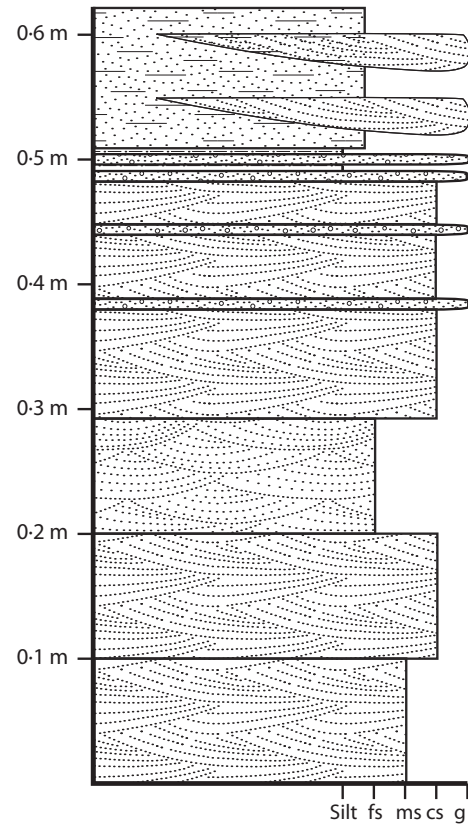

Fig. 15. Stratigraphy observed at the south-west end of the outcrop. The section is dominated by stacked sets of trough cross-bedding. Several coarse-grained outcrop-length surfaces are visible higher up in the section. Bedsets at the top of the outcrop, comprising Unit 3, consist of a fine-grained well-laminated facies with lenses of coarse-grained sandstones. Grain sizes are denoted on the right-hand side of the column, including silt, fine-sand (fs), medium sand (ms), coarse sand (cs) and gravel (g).

Each of these surfaces is commonly overlain by a basal granule and fine pebble-rich bed that fines upward into sandstone (Fig. 16A, inset). The surfaces exhibit a sharp sub-planar geometry; no evidence for erosional scour is observed. Mastcam stereo data indicate that the surfaces dip approximately 10 to 15° towards the south-east quadrant and are also slightly concave in planform towards the south-east (Fig. 12). The surfaces enable the sub-division of Unit 2 into four distinct packages that contain Facies 4, 5 and 6 (Fig. 16A). The packages show both lateral and vertical changes in grain size and sedimentary structures. Each package is from several centimetres to 10 cm in thickness. At the south-west end of the main outcrop, Unit 2 is dominated by Facies 6, which comprises stacked

planar-bedded and trough cross-bedded pebbly sandstones (Fig. 13D). The cross-bedded sandstones are superimposed on larger-scale dipping surfaces, forming compound cross-stratification (Banks, 1973; Rubin & Carter, 2006). Unit 2 shows an increase in heterolithic facies traced from south-west to north-east with a greater proportion of finer-grained facies towards the north-east, suggesting an overall fining to the north-eastern part of the outcrop. In general, cross-bedding suggests flow towards the north-east. In the main part of Unit 2, sediment packages show a fining-up signature from granule-rich basal beds through well-developed cross-stratified sandstone into recessively weathered beds and covered intervals inferred to be finer-grained (Fig. 16A).

Interpretation

Each sediment package is interpreted to represent a single flow event involving initial granule deposition, followed by bedform migration, and terminated by possible suspension fallout at lower flow velocities. Each fining-upward succession thus may record deposition during a waning flow. At the south-western part of the outcrop, the stacking of bedsets records aggradation of dune-formed strata. Here, the occurrence of compound cross-stratification also indicates the superposition of dunes on larger inclined surfaces. Cross-bed dip directions suggest that superimposed dunes migrated to the north-east, on surfaces that were inclined towards the east/north-east.

Unit 3

The uppermost part of the Shaler outcrop is distinctly different from the main body of Shaler and is inferred to record a change in the sedimentary system. Unit 3 forms a sheet-like tabular bed at outcrop scale (Fig. 7). It is *ca* 20 m in lateral extent and varies between *ca* 10 cm and 20 cm in thickness, being thickest at its south-western limit. It has an aspect ratio (W/H) of 100. Unit 3 overlies recessive weathering, probably fine-grained sediments of Unit 2 (Figs 7A and 16A). The basal contact is not exposed but probably forms a sharp boundary. At its south-western end, the unit is thicker and appears to infill erosional topography in underlying units (Fig. 7C). There is a coarser-grained wedge at the south-western end of the outcrop. The two sedimentary subfacies in Unit 3 appear to be interstratified across the outcrop

(Fig. 7B and C). At the south-west end of the outcrop, Unit 3 shows a succession that consists of: (i) fine-grained, smooth, well-laminated sandstone (Facies 7B) at the base; overlain by (ii) coarser-grained, vuggy, cross-stratified sandstone (Facies 7A); overlain by (iii) a covered, probably more recessive interval; followed by (iv) another coarse-grained, vuggy, cross-stratified sandstone (Facies 7A); followed by (v) laminated sandstone (Facies 7B). The middle coarse sub-units laterally pinch out north-eastward over several metres (Figs 7C and 14). Although cross-bedding is visible in places, there is insufficient intact exposure to enable palaeocurrent analyses.

Interpretation

Unit 3 records flows of variable strength extending across the length of the outcrop. The high aspect ratio of the sandbody and prevalence of planar lamination are consistent with deposition as a non-channelized fluvial deposit (Fisher *et al.*, 2007). Because of the distinct change in facies in Unit 3 compared to the rest of the Shaler outcrop and the distinct geochemistry of Unit 3 which suggests that it is enriched in K_2O (McLennan *et al.*, 2014; Anderson *et al.*, 2015), the unit is interpreted to record the abrupt transition to a new sedimentary system characterized by a distinct provenance; this suggests that the fluvial system represented by the lower part of the outcrop was replaced by the dispersal system represented by Unit 3.

DISCUSSION

Palaeomorphology of the Shaler fluvial deposits

The grain size, texture and sedimentary structures displayed by the Shaler outcrop lead to the interpretation that the sandbody is a fluvial deposit, arguably the best characterized *in situ* fluvial strata observed on Mars. Despite the small size of the outcrop, its heterogeneity is quite remarkable, which allows for the description of subtle sedimentary features. Grain-size analysis of Shaler indicates that the sedimentary deposits contain granule and fine pebble sizes (up to 5 mm in diameter). While there are significant unknowns about the thickness of the past Mars atmosphere and the wind friction speed required to initiate particle motion (cf. Pollack *et al.* 1976), the grain size of the largest clasts is
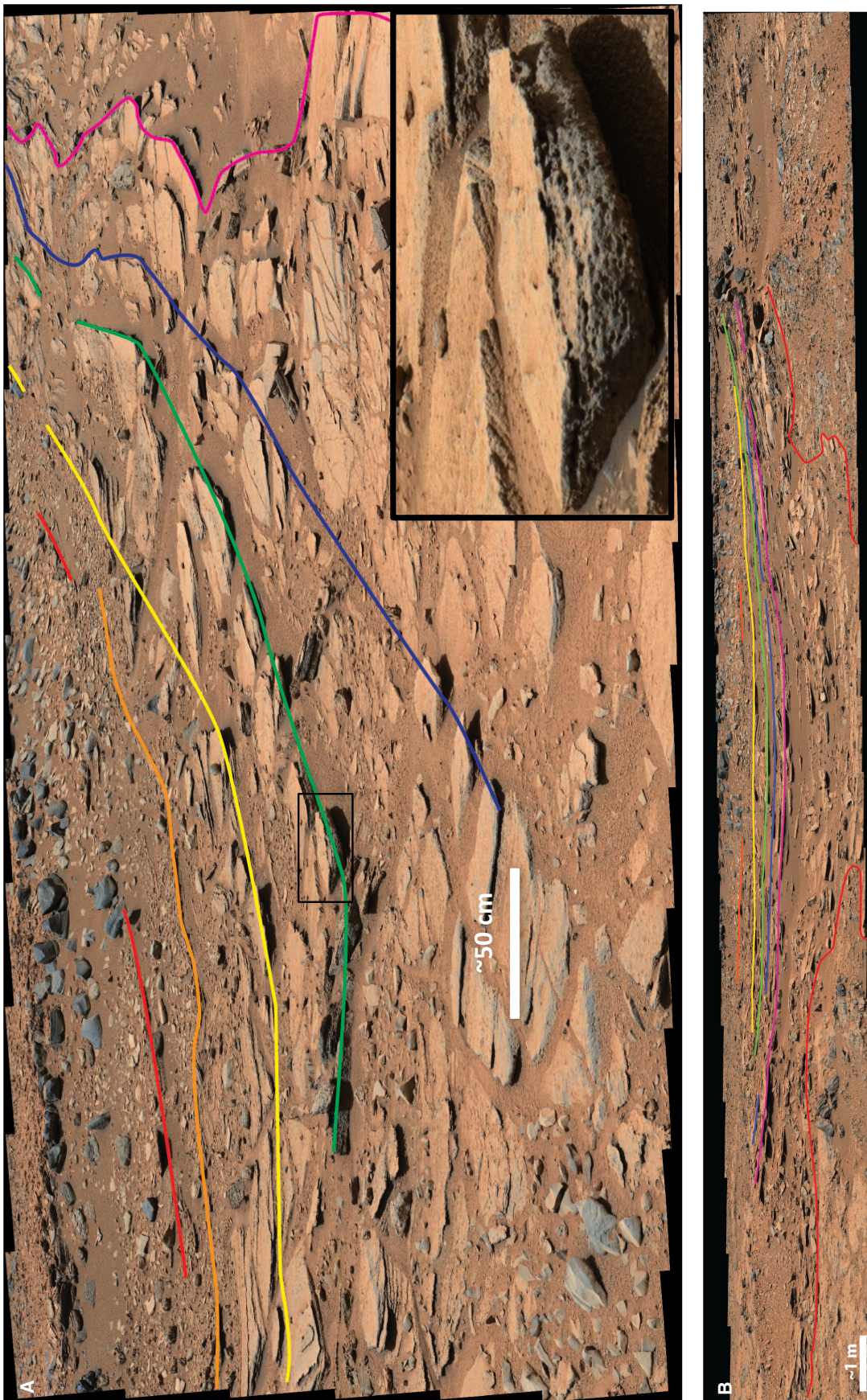
Fig. 16. (A) Mastcam mosaics from multiple viewing geometries enable the identification of several outcrop-length surfaces, shown here by the different coloured lines. These surfaces allow correlation of distinct sediment packages across the outcrop. Mastcam stereo data indicate that these surfaces dip *ca* 10 to 15° to the south-east (into the page). Inset shows a close-up of one of these surfaces defined by gravel-rich beds which fine upward. Mastcam mosaic acquired on Sol 309 by the M100 camera, mcam01275. Image credit: NASA/JPL-Caltech/MSSS. (B) Outcrop-length surfaces traced across the full width of the Shaler outcrop. Red line at the base indicates the contact with the underlying Gillespie sandstone. Mastcam mosaic acquired by the M100 camera on Sol 120, mcam00752. Image credit: NASA/JPL-Caltech/MSSS.

probably too large to have been transported substantial distances by aeolian processes (Williams *et al.*, 2013; Grotzinger *et al.*, 2014), thus indicating that the Shaler bedsets largely represent deposition from fluvial flows. Moreover, the relatively poor sorting of the sandstones and variability of grain shape from subrounded to subangular are more consistent with fluvial sediment transport and deposition than aeolian processes. The abundance of trough cross-stratified individual sets or stacked cosets indicates bedload sediment transport by migration of subaqueous sinuous crested dunes. The dominance of cross-stratification and the general absence of upper flow regime sedimentary structures such as upper stage plane beds may suggest brief periods of sustained flow rather than a regime with highly variable discharge (Fielding, 2006; Ielpi & Ghinassi, 2015).

The limited spatial extent of the Shaler outcrop prevents reconstruction of the large-scale morphology of the palaeo-fluvial system that Shaler formed part of. Nevertheless, the wealth of sedimentological features observed in the outcrop enables interpretation of the fluvial depositional morphology that Shaler is likely to represent. The Shaler outcrop is dominated at a large scale by beds that dip *ca* 10 to 15° to the south-east. These beds, which are bounded by larger-scale inclined surfaces that can be traced across the outcrop, are interpreted to record accretion of sedimentary layers on a larger-scale fluvial barform. In plain view, this barform had a subtle south-east-facing concavity, and sedimentary layers accreted towards the south-east.

Although large-scale bar accretion was to the south-east, individual bedsets show two contrasting characteristics. At the south-western section of the outcrop, the bedsets comprise stacked compound cross-bed sets (Facies 6) (Fig. 13D). The cross-sets indicate palaeoflow approximately to the north-east, perpendicular to the large-scale dip of bedsets that define bar topography. These sets are interpreted to have formed by trains of superimposed fluvial dunes that migrated across the bar topography. The stacked cross-beds probably represent bar core facies. Traced north-eastward, the stacked cross-beds transition to a more heterolithic facies succession characterized by individual fining-up bedsets that comprise a basal granule – fine pebble lag overlain by an isolated cross-bed set (Fig. 13A and C). These isolated sets record migration and deposition from episodes of dune migration (Facies 5). The presence of a basal gravel lag and the fining-up character of these bedsets suggest episodic flow events on the bar surface (Fig. 16A).
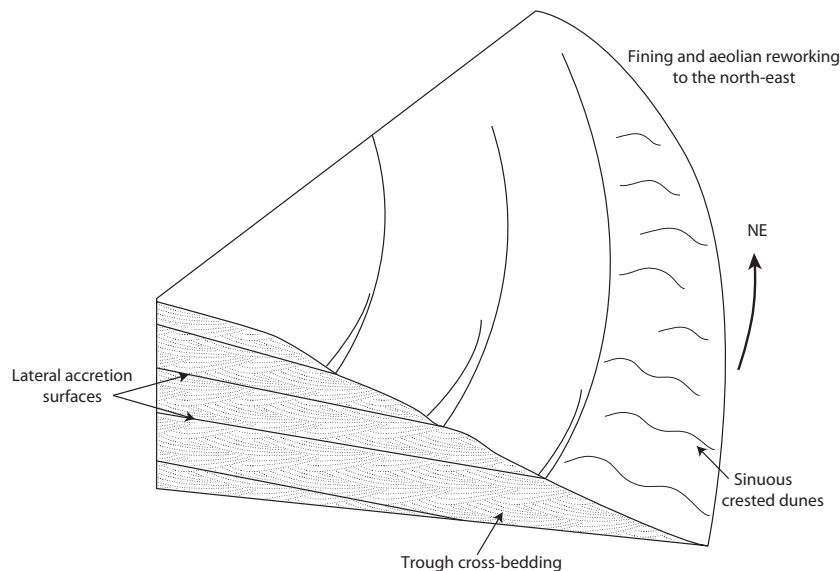
Fig. 17. Schematic diagram of a fluvial bar as a model for the Shaler outcrop. Large-scale surfaces dip to the south-east (to the right in the above figure), recording bar accretion to the south-east. Superimposed bedforms migrated primarily to the north-east, in the direction of the local flow. Finer grain sizes and aeolian reworking are observed at the north-eastern end of the bar. Note that the diagram is intended as a schematic to illustrate certain aspects of the Shaler outcrop, but does not capture the slight concavity recorded by the large-scale lateral accretion surfaces.

Overall, in the context of a fluvial bar, the large-scale surfaces record incremental lateral accretion to the south-east, while the superimposed bedforms record flow to the north-east (Fig. 17). The observed large-scale grain size fining from the south-west to the north-east section of the outcrop may be related to downflow transition from deposition on the central core of a bar to its downstream flanks.

It remains difficult to determine the exact depositional setting of the bar topography at Shaler. Although the geometries observed suggest lateral accretion on a barform, the lack of extensive exposure prevents the distinction as to whether the Shaler bedsets represent part of a bank-attached barform or part of a mid-channel bar developed in a braided fluvial system. Nevertheless, the observations and interpretations presented here represent a major advance in reconstructing fluvial depositional geometries on another planet.

Depositional evolution, sediment dispersal patterns and palaeogeography

The Shaler outcrop stratigraphically overlies the Gillespie Lake member. Mapping of the basal contact reveals that lowermost Unit 1 Shaler bedsets drape subtle palaeotopographic variations on the upper surface of the Gillespie Lake sandstone (Fig. 5C and D). This transition represents a distinct change in depositional environment from distal fan fluvial deposits to more proximal fluvial deposits, suggesting basinward progradation of the fluvial system through time. The identification of distinct depositional signatures along the outcrop trace in the lowermost part of Shaler suggests that the base of the section was compartmentalized, which suggests the presence of palaeotopography on the basal surface.

Analysis of bedding dip relationships, cross-stratification, grain-size trends and provenance relations from geochemistry enables the reconstruction of approximate palaeo-transport patterns. Large-scale bedding dips traced across the outcrop indicate dips to the south-east, which probably represent inclined surfaces on a fluvial bar that accreted to the south-east. Palaeo-flow directions obtained from small-scale cross-stratification formed by migrating dunes indicate flows predominantly to the north-east. However, at the base of the section, more variability in flow direction is observed. Thus, the local palaeoflow direction along the bar that deposited the Shaler fluvial system was approximately from south-west to north-east. Due to the limited exposure of the Shaler outcrop, it is not possible to place further constraints on the spatial extent of the Shaler fluvial system. Moreover, because fluvial systems can show marked local variability in orientation of channels and flow directions from one site to another – either as observed in a river or inferred from cross-strata deposited by small-scale bedforms – the south-west to north-east orientation inferred at the outcrop does not necessarily represent a regional transport direction.

The top of the Shaler outcrop records an abrupt transition to a new fluvial dispersal system characterized by a distinct change in sedimentary character and provenance. Unlike the platy nature of beds in the lower part of Shaler (Units 1 and 2), the uppermost beds in the outcrop (Unit 3) are smoother weathering, more resistant to erosion and have a blocky character. ChemCam geochemical analyses show that Unit 3 is enriched in K_2O; this has been inferred to represent derivation from an alkaline igneous source (Anderson *et al.*, 2015; Mangold *et al.*, 2015). The sedimentological and geochemical evidence for a distinct change across the transition from Units 1 and 2 of the Shaler outcrop into Unit 3 implies a relatively abrupt change in depositional morphology and provenance. The source region of the Yellowknife Bay formation has been interpreted to be the Gale crater rim, which probably had heterogeneous bedrock geological units exposed in its catchments. The abrupt transition to Unit 3 may record either exhumation of a new bedrock unit characterized by alkaline igneous rocks during progressive erosion of the crater rim, or a drainage capture event that tapped a new alkaline igneous source. The fact that the transition in geochemical properties matches a change in sedimentary character lends credence to a model invoking initiation of a new sediment dispersal system at this stratigraphic transition. Absence of outcrop control prevents reconstruction of stratigraphic relationships with strata that overlie the Shaler outcrop.

The Shaler outcrop occurs stratigraphically in the upper part of the Yellowknife Bay formation succession, above the Sheepbed lacustrine mudstones and Gillespie Lake distal fan fluvial sandstones (Grotzinger *et al.*, 2014). The coarser grain sizes observed in the Shaler outcrop indicate that the succession forms part of an overall coarsening-up succession. Given the overall fluvial fan to lake context of the Yellowknife Bay formation (Grotzinger *et al.*,

2014), the Shaler outcrop probably represents basinward progradation of a fluvial system derived from the crater rim and infilling of a palaeo-basin in Gale crater. The presence of subrounded granules and fine pebbles, and moderate to good sorting in the sandstone facies suggest that grains were transported over a sufficient distance to attain some degree of rounding and become sorted hydraulically. The Yellowknife Bay formation crops out at the distal part of the Peace Vallis alluvial fan system, which is sourced from the northern crater rim (Palucis *et al.*, 2014). Current surface topography indicates that the downslope direction of the fan is towards the south-east, and numerous inverted channels on the western portion of the fan are consistent with a southward transport direction (Palucis *et al.*, 2014). The palaeo-flow directions within the Shaler outcrop are somewhat at variance with the more regional indicators; this is likely to be a result of local variance in flow azimuth.

The relationship of the Peace Vallis fan system to the Yellowknife Bay formation is currently unresolved (Stack & Grotzinger, 2015). In one model, the Yellowknife Bay formation represents distal and time equivalent rocks to the Peace Vallis fan (Sumner *et al.*, 2015). Alternatively, the Yellowknife Bay formation may represent the distal part of a stratigraphically older fan system, although representing a similar type of sedimentary system to the Peace Vallis sediment dispersal system (Grotzinger *et al.*, 2014).

Implications for habitable environments and Martian climate

The goal of the MSL mission is to explore and quantitatively assess habitable environments on Mars. One of the key factors in the search for habitable environments is evidence for sustained liquid water on the surface of Mars. At Gale crater, a habitable environment was identified at Yellowknife Bay, with the discovery of fine-grained lacustrine mudstones of the Sheepbed member, although these deposits were relatively thin (Grotzinger *et al.*, 2014).

Strata of the Shaler outcrop stratigraphically overlie and are therefore younger than the Sheepbed mudstone. Sedimentary structures preserved in the outcrop provide strong evidence for episodes of sustained flows of liquid water at the Martian surface. Although fluvial environments are not ideal settings for the preservation of organic matter (Summons *et al.*,

2011), the Shaler fluvial system may have fed water and sediment to a downstream stratigraphically equivalent lacustrine system; thus, it is plausible that thicker lake deposits that are now eroded may have existed in the Yellowknife Bay area.

Sedimentological evidence suggests sustained water flow throughout deposition of the Yellowknife Bay formation. Sustained flowing water requires a more humid climate, which suggests that the climate conditions that existed during deposition of the Yellowknife Bay formation in the Early Hesperian (Grotzinger *et al.*, 2015) must have been different from the cold, arid conditions that exist on Mars today. However, current climate models have difficulty modelling clement conditions for any extended length of time beginning from the earliest period of Martian history to the present day (Haberle *et al.*, 2001, 2015). The discrepancy between sedimentological observations that indicate the sustained presence of aqueous environments and climate models that predict arid conditions throughout Mars' history (Haberle *et al.*, 2015) suggests a need for improved integration of these two different data sets.

CONCLUSIONS

The Shaler outcrop of the Glenelg member (Yellowknife Bay formation) represents the first opportunity to reconstruct at fine-scale the sedimentary architecture and palaeo-morphology of a fluvial environment on Mars. Through identification of sedimentary facies, reconstruction of outcrop-scale architecture, and analyses of bedforms and palaeoflow indicators, the following conclusions are drawn:

1 The Shaler outcrop is shown to comprise deposits infilling three shallow palaeodepressions incised into the underlying fluvial sandstones of the Gillespie Lake member.
2 Classification of the Shaler outcrop into seven different sedimentary facies provides insight into spatial and temporal variation in depositional processes and sedimentary provenance.
3 Grain-size analyses indicate that the deposits incorporate grains up to granule and fine pebble sizes (up to *ca* 5 mm in diameter) and that these grains are subrounded. Grain-size measurements indicate that the majority of the Shaler deposit is probably too coarse-grained to have been

transported by aeolian processes. Cross-bedded facies are thus interpreted as the deposits of subaqueous dunes formed in a fluvial environment.

4 Cross-bed sets occur as individual sets or as stacked cosets. The stacked cosets suggest aggradation of multiple bedforms, which provides clear evidence for short periods of sustained flow during Shaler deposition. However, local evidence for aeolian reworking and the presence of possible desiccation cracks suggests that fluvial deposition may have been intermittently interrupted.

5 The identification of several surfaces that can be traced across the entire length of the outcrop permits correlation of bedsets and reconstruction of spatial variation in facies architecture. Analysis of the large-scale geometry of bedsets indicates that outcrop-length surfaces dip *ca* 10 to 15° to the south-east (which is in contrast to flow directions indicated by cross-bed sets formed by dune migration) which suggests accretion of large-scale bedsets towards the south-east.

6 While the larger-scale bar feature accreted to the south-east, sinuous crested dunes migrated across its surface, depositing cross-bed sets characterized by trough cross-bedding. Unidirectional flow further supports a fluvial interpretation.

7 On the basis of bedform migration direction, grain-size distribution and large-scale morphology (south-east-facing concavity), this study concludes that the Shaler outcrop is likely to record the accretion of a fluvial barform. Flow along the accreting flank of the bar was from south-west to north-east. This flow direction is interpreted to represent local variance within a more extensive fluvio-lacustrine system that prograded southward from the Gale crater rim.

8 The uppermost bedsets at the Shaler outcrop are distinctly different in terms of texture and chemistry compared to underlying bedsets, and are inferred to record deposition from a sediment dispersal system with a different provenance.

9 The abundance of cross-stratified bedsets recording migration of fluvial dunes within Shaler is clear evidence of sustained surface water flow in a depositional fluvial system. In combination with observations of lacustrine mudstones and distal fluvial sandstones within the Yellowknife Bay formation, the fluvial deposits of the Shaler outcrop provide evidence for multiple aqueous environments, and the presence of liquid water flow on the surface of Mars in the Early Hesperian.

REFERENCES

Anderson, R., Bridges, J.C., Williams, A., Edgar, L., Ollila, A., Williams, J., Nachon, M., Mangold, N., Fisk, M., Schieber, J., Gupta, S., Dromart, G., Wiens, R., Le Mouélic, S., Forni, O., Lanza, N., Mezzacappa, A., Sautter, V., Blaney, D., Clark, B., Clegg, S., Gasnault, O., Lasue, J., Léveillé, R., Lewin, E., Lewis, K.W., Maurice, S., Newsom, H., Schwenzer, S.P. and Vaniman, D. (2015) ChemCam results from the Shaler outcrop in Gale crater, Mars. *Icarus*, **249**, 2–21.

Baker, V.R., Hamilton, C.W., Burr, D.M., Gullick, V.C., Komatsu, G., Luo, W., Rice, J.W. and Rodriguez, J.A.P. (2015) Fluvial geomorphology on Earth-like planetary surfaces: a review. *Geomorphology*, **245**, 149–182.

Banks, N.L. (1973) Origin and significance of some downcurrent-dipping cross-stratified sets. *J. Sed. Petrol.*, **43**, 423–427.

Burr, D.M., Williams, R.M.E., Wendell, K.D., Chojnacki, M. and Emery, J.P. (2010) Inverted fluvial features in the Aeolis/Zephyria Plana region, Mars: formation mechanism and initial paleodischarge estimates. *J. Geophys. Res. Planets*, **115**, E07011.

Cabrol, N.A., Grin, E.A., Newsom, H.E., Landheim, R. and McKay, C.P. (1999) Hydrogeologic evolution of gale crater and its relevance to the exobiological exploration of Mars. *Icarus*, **139**, 235–245.

Calef, F.J.I., Dietrich, W.E., Edgar, L., Farmer, J., Fraeman, A., Grotzinger, J., Palucis, M.C., Parker, T., Rice, M., Rowland, S., Stack, K.M., Sumner, D., Williams, J. and Team, M.S. (2013) Geologic mapping of the Mars science laboratory landing ellipse. 44th Lunar and Planet. Sci. Conf., abstract 2511.

Carr, M.H. and Head III, J.W. (2010) Geologic history of Mars. *Earth and Planetary Science Letters*, Mars Express after 6 Years in Orbit: Mars Geology from Three-Dimensional Mapping by the High Resolution Stereo Camera (HRSC) Experiment **294**, 185–203. doi:10.1016/j.epsl.2009.06.042

DiBiase, R.A., Limaye, A.B., Scheingross, J.S., Fischer, W.W. and Lamb, M.P. (2013) Deltaic deposits at Aeolis Dorsa: sedimentary evidence for a standing body of water on the northern plains of Mars. *J. Geophys. Res. Planets*, **118**, 1285–1302.

Dott, R.H. (1973) Paleocurrent analysis of trough cross stratification. *J. Sed. Petrol.*, **43**, 779–783.

Edgar, L.A., Rubin, D.M., Grotzinger, J.P., Bell, J.F., Calef, F.J., Dromart, G., Gupta, S., Kah, L.C., Lewis, K.W.,

Mangold, N., Schieber, J., Stack, K.M., Sumner, D.Y. and MSL Science Team (2013) Sedimentary Facies and Bedform Analysis Observed from the Rocknest Outcrop (Sols 59-100), Gale Crater, Mars. 44th Lunar and Planet. Sci. Conf., abstract 1628.

Edgett, K.S., Yingst, R.A., Ravine, M.A., Caplinger, M.A., Maki, J.N., Ghaemi, F.T., Schaffner, J.A., Bell III, J.F., Edwards, L.J., Herkenhoff, K.E., Heydari, E., Kah, L.C., Lemmon, M.T., Minitti, M.E., Olson, T.S., Parker, T.J., Rowland, S.K., Schieber, J., Sullivan, R.J., Sumner, D.Y., Thomas, P.C., Jensen, E.H., Simmonds, J.J., Sengstacken, A.J., Willson, R.G. and Goetz, W. (2012) Curiosity's Mars Hand Lens Imager (MAHLI) investigation. *Space Sci. Rev.*, **170**, 259–317.

Fielding, C.R. (2006) Upper flow regime sheets, lenses and scour fills: extending the range of architectural elements for fluvial sediment bodies. *Sed. Geol.*, **190**, 227–240.

Fisher, J.A., Nichols, G.J. and Waltham, D.A. (2007) Unconfined flow deposits in distal sectors of fluvial distributary systems: examples from the Miocene Luna and Huesca Systems, northern Spain. *Sed. Geol.*, **195**, 55–73.

Fryberger, S.G. and Schenk, C.J. (1988) Pin stripe lamination: a distinctive feature of modern and ancient eolian sediments. *Sed. Geol.*, **55**, 1–15.

Goddard, K., Warner, N.H., Gupta, S. and Kim, J.R. (2014) Mechanisms and timescales of fluvial activity at Mojave and other young Martian craters. *J. Geophys. Res. Planets*, **119**, 604–634.

Grant, J.A., Wilson, S.A., Mangold, N., Calef, F. and Grotzinger, J.P. (2014) The timing of alluvial activity in Gale crater, Mars. *Geophys. Res. Lett.*, **41**, 2013GL058909.

Grotzinger, J., Beaty, D., Dromart, G., Gupta, S., Harris, M., Hurowitz, J., Kocurek, G., McLennan, S., Milliken, R., Ori, G.G. and Sumner, D. (2011) Mars sedimentary geology: key concepts and outstanding questions. *Astrobiology*, **11**, 77–87.

Grotzinger, J.P., Gupta, S., Malin, M.C., Rubin, D.M., Schieber, J., Siebach, K., Sumner, D.Y., Stack, K.M., Vasavada, A.R., Arvidson, R.E., Calef, F., Edgar, L., Fischer, W.F., Grant, J.A., Griffes, J., Kah, L.C., Lamb, M.P., Lewis, K.W., Mangold, N., Minitti, M.E., Palucis, M., Rice, M., Williams, R.M.E., Yingst, R.A., Blake, D., Blaney, D., Conrad, P., Crisp, J., Dietrich, W.E., Dromart, G., Edgett, K.S., Ewing, R.C., Gellert, R., Hurowitz, J.A., Kocurek, G., Mahaffy, P., McBride, M.J., McLennan, S.M., Mischna, M., Ming, D., Milliken, R., Newsom, H., Oehler, D., Parker, T.J., Vaniman, D., Wiens, R.C. and Wilson, S.A. (2015) Deposition, exhumation, and paleoclimate of an ancient lake deposit, Gale crater, Mars. *Science*, **350**, aac7575.

Grotzinger, J.P., Sumner, D.Y., Kah, L.C., Stack, K., Gupta, S., Edgar, L., Rubin, D., Lewis, K., Schieber, J., Mangold, N., Milliken, R., Conrad, P.G., DesMarais, D., Farmer, J., Siebach, K., Calef, F., Hurowitz, J., McLennan, S.M., Ming, D., Vaniman, D., Crisp, J., Vasavada, A., Edgett, K.S., Malin, M., Blake, D., Gellert, R., Mahaffy, P., Wiens, R.C., Maurice, S., Grant, J.A., Wilson, S., Anderson, R.C., Beegle, L., Arvidson, R., Hallet, B., Sletten, R.S., Rice, M., Bell, J., Griffes, J., Ehlmann, B., Anderson, R.B., Bristow, T.F., Dietrich, W.E., Dromart, G., Eigenbrode, J., Fraeman, A., Hardgrove, C., Herkenhoff, K., Jandura, L., Kocurek, G., Lee, S., Leshin, L.A., Leveille, R., Limonadi, D., Maki, J., McCloskey, S., Meyer, M., Minitti, M., Newsom, H., Oehler, D., Okon, A., Palucis, M., Parker, T., Rowland, S., Schmidt, M., Squyres, S., Steele, A., Stolper, E.,

Summons, R., Treiman, A., Williams, R., Yingst, A. and Team, M.S. (2014) A Habitable fluvio-lacustrine environment at Yellowknife bay, gale crater, Mars. *Science*, **343**, 1242777.

Haberle, R.M., McKay, C.P., Schaeffer, J., Cabrol, N.A., Grin, E.A., Zent, A.P. and Quinn, R. (2001) On the possibility of liquid water on present-day Mars. *J. Geophys. Res.*, **106**, 23317–23326.

Haberle, R.M., Carr, M.H., Catling, D.C. and Zahnle, K. (2015) The early Mars climate system. In: *The Atmosphere and Climate of Mars*, pp. 23317–23326. Cambridge University Press.

Herbert, C.M., Alexander, J. and Martínez de Álvaro, M.J. (2015) Back-flow ripples in troughs downstream of unit bars: Formation, preservation and value for interpreting flow conditions. *Sedimentology*, **62**, 1814–1836.

High, L.R. and Picard, M.D. (1974) Reliability of cross-stratification types as paleocurrent indicators in fluvial rocks. *J. Sed. Petrol.*, **44**, 158–168.

Hunter, R.E. (1977a) Basic types of stratification in small eolian dunes. *Sedimentology*, **24**, 361–387.

Hunter, R.E. (1977b) Terminology of cross-stratified sedimentary layers and climbing-ripple structures. *J. Sed. Petrol.*, **47**, 697–706.

Ielpi, A. and Ghinassi, M. (2015) Planview style and palaeodrainage of Torridonian channel belts: applecross Formation, Stoer Peninsula, Scotland. *Sed. Geol.*, **325**, 1–16.

Irwin, R.P., Howard, A.D., Craddock, R.A. and Moore, J.M. (2005) An intense terminal epoch of widespread fluvial activity on early Mars: 2. Increased runoff and paleolake development. *J. Geophys. Res.*, **110**, E12S15.

Jacob, S.R., Rowland, S., Calef III, F.J., Stack, K.M. and Team, M. (2014) Characteristics and origin of a cratered unit near the MSL Bradbury landing site (Gale Crater, Mars) based on analyses of surface data and orbital imagery. 43rd Lunar and Planet. Sci. Conf., abstract 1395.

Kite, E.S., Howard, A.D., Lucas, A.S., Armstrong, J.C., Aharonson, O. and Lamb, M.P. (2015) Stratigraphy of Aeolis Dorsa, Mars: stratigraphic context of the great river deposits. *Icarus*, **253**, 223–242.

Le Deit, L., Hauber, E., Fueten, F., Pondrelli, M., Rossi, A.P. and Jaumann, R. (2013) Sequence of infilling events in Gale Crater, Mars: Results from morphology, stratigraphy, and mineralogy. *J. Geophys. Res. Planets*, **118**, 2012JE004322.

Le Mouelic, S., Gasnault, O., Herkenhoff, K.E., Bridges, N.T., Langevin, Y., Mangold, N., Maurice, S., Wiens, R.C., Pinet, P., Newsom, H.E., Deen, R.G., Bell III, J.F., Johnson, J.R., Rapin, W., Barraclough, B., Blaney, D.L., Deflores, L., Maki, J., Malin, M.C., Perez, R. and Saccoccio, M. (2015) The ChemCam Remote Micro-Imager at Gale crater: review of the first year of operations on Mars. *Icarus*, **249**, 93–107.

Maki, J., Thiessen, D., Pourangi, A., Kobzeff, P., Litwin, T., Scherr, L., Elliott, S., Dingizian, A. and Maimone, M. (2012) The mars science laboratory engineering cameras. *Space Sci. Rev.*, **170**, 77–93.

Malin, M.C. and Edgett, K.S. (2003) Evidence for persistent flow and aqueous sedimentation on early Mars. *Science*, **302**, 1931–1934.

Malin, M.C., Caplinger, M.A., Edgett, K.S., Ghaemi, F.T., Ravine, M.A., Schaffner, J.A., Baker, J.M., Bardis, J.D., Dibiase, D.R., Maki, J.N., Willson, R.G., Bell, J.F.,

Dietrich, W.E., Edwards, L.J., Hallet, B., Herkenhoff, K.E., Heydari, E., Kah, L.C., Lemmon, M.T., Minitti, M.E., Olson, T.S., Parker, T.J., Rowland, S.K., Schieber, J., Sullivan, R.J., Sumner, D.Y., Thomas, P.C. and Yingst, R.A. (2010) The Mars Science Laboratory (MSL) Mast-mounted Cameras (Mastcams) Flight Instruments. 41st Lunar and Planet. Sci. Conf., abstract 1123.

Mangold, N., Forni, O., Dromart, G., Stack, K., Wiens, R.C., Gasnault, O., Sumner, D.Y., Nachon, M., Meslin, P.Y., Anderson, R.B., Barraclough, B., Bell III, J.F., Berger, G., Blaney, D.L., Bridges, J.C., Calef, F., Clark, B., Clegg, S.M., Cousin, A., Edgar, L., Edgett, K., Ehlmann, B., Fabre, C., Fisk, M., Grotzinger, J., Gupta, S., Herkenhoff, K.E., Hurowitz, J., Johnson, J.R., Kah, L.C., Lanza, N., Lasue, J., Le Mouelic, S., Leveille, R., Lewin, E., Malin, M., McLennan, S., Maurice, S., Melikechi, N., Mezzacappa, A., Milliken, R., Newsom, H., Ollila, A., Rowland, S.K., Sautter, V., Schmidt, M., Schroeder, S., d'Uston, C., Vaniman, D. and Williams, R. (2015) Chemical variations in Yellowknife Bay formation sedimentary rocks analyzed by ChemCam on board the Curiosity rover on Mars. *J. Geophys. Res. Planets*, **120**, 452–482.

Martinius, A.W. and Van den Berg, J.H. (2011) *Atlas of Sedimentary Structures in Estuarine and Tidally-Influenced River Deposits of the Rhine Meuse-Scheldt System.* European Association of Geoscientists & Engineers, Houten, Netherlands. 298 pp.

Maurice, S., Wiens, R.C., Saccoccio, M., Barraclough, B., Gasnault, O., Forni, O., Mangold, N., Baratoux, D., Bender, S., Berger, G., Bernardin, J., Berthe, M., Bridges, N., Blaney, D., Bouye, M., Cais, P., Clark, B., Clegg, S., Cousin, A., Cremers, D., Cros, A., DeFlores, L., Derycke, C., Dingler, B., Dromart, G., Dubois, B., Dupieux, M., Durand, E., d'Uston, L., Fabre, C., Faure, B., Gaboriaud, A., Gharsa, T., Herkenhoff, K., Kan, E., Kirkland, L., Kouach, D., Lacour, J.L., Langevin, Y., Lasue, J., Le Mouelic, S., Lescure, M., Lewin, E., Limonadi, D., Manhes, G., Mauchien, P., McKay, C., Meslin, P.Y., Michel, Y., Miller, E., Newsom, H.E., Orttner, G., Paillet, A., Pares, L., Parot, Y., Perez, R., Pinet, P., Poitrasson, F., Quertier, B., Salle, B., Sotin, C., Sautter, V., Seran, H., Simmonds, J.J., Sirven, J.B., Stiglich, R., Striebig, N., Thocaven, J.J., Toplis, M.J. and Vaniman, D. (2012) The ChemCam instrument suite on the Mars Science Laboratory (MSL) rover: science objectives and mast unit description. *Space Sci. Rev.*, **170**, 95–166.

McLennan, S.M., Anderson, R.B., Bell, J.F., Bridges, J.C., Calef, F., Campbell, J.L., Clark, B.C., Clegg, S., Conrad, P., Cousin, A., Des Marais, D.J., Dromart, G., Dyar, M.D., Edgar, L.A., Ehlmann, B.L., Fabre, C., Forni, O., Gasnault, O., Gellert, R., Gordon, S., Grant, J.A., Grotzinger, J.P., Gupta, S., Herkenhoff, K.E., Hurowitz, J.A., King, P.L., Mouélic, S., Leshin, L.A., Léveillé, R., Lewis, K.W., Mangold, N., Maurice, S., Ming, D.W., Morris, R.V., Nachon, M., Newsom, H.E., Ollila, A.M., Perrett, G.M., Rice, M.S., Schmidt, M.E., Schwenzer, S.P., Stack, K., Stolper, E.M., Sumner, D.Y., Treiman, A.H., VanBommel, S., Vaniman, D.T., Vasavada, A., Wiens, R.C. and Yingst, R.A. (2014) Elemental geochemistry of sedimentary rocks at Yellowknife Bay, Gale Crater, Mars. *Science*, **343**, 1244734.

Michelson, P.C. and Dott, R.H. (1973) Orientation analysis of trough cross stratification in upper Cambrian sandstones of western Wisconsin. *J. Sed. Petrol.*, **43**, 784–794.

Moore, J.M. and Howard, A.D. (2005) Large alluvial fans on Mars. *J. Geophys. Res. Planets*, **110**, E04005.

Owen, G. and Moretti, M. (2011) Identifying triggers for liquefaction-induced soft-sediment deformation in sands. *Sed. Geol.*, **235**, 141–147.

Owen, G. and Santos, M.G.M. (2014) Soft-sediment deformation in a pre-vegetation river system: the Neoproterozoic Torridonian of NW Scotland. *Proc. Geol. Assoc.*, **125**, 511–523.

Owen, G., Moretti, M. and Alfaro, P. (2011) Recognising triggers for soft-sediment deformation: current understanding and future directions. *Sed. Geol.*, **235**, 133–140.

Palucis, M.C., Dietrich, W.E., Hayes, A.G., Williams, R.M.E., Gupta, S., Mangold, N., Newsom, H., Hardgrove, C., Calef III, F. and Sumner, D.Y. (2014) The origin and evolution of the Peace Vallis fan system that drains to the Curiosity landing area, Gale Crater, Mars. *J. Geophy. Res. Planets*, **119**, 705–728.

Pollack, J.B., Haberle, R., Greeley, R. and Iversen, J. (1976) Estimates of the wind speeds required for particle motion on Mars. *Icarus*, **29**, 395–417.

Rice, M.S., Gupta, S., Bell III, J.F. and Warner, N.H. (2011) Influence of fault-controlled topography on fluvio-deltaic sedimentary systems in Eberswalde crater, Mars. *Geophys. Res. Lett.*, **38**, L16203.

Rubin, D.M. and Carter, C.L. (2006) Cross-bedding, bedforms, and paleocurrents. In: *SEPM Concepts in Sedimentology and Paleontology* (Ed. B.H. Lidz) 2nd edn, **1**, pp. 195.

Schieber, J., Bish, D., Coleman, M., Reed, M., Hausrath, E.M., Cosgrove, J., Gupta, S., Minitti, M.E., Edgett, K.S. and Malin, M. (2017) Encounters with an unearthly mudstone: Understanding the first mudstone found on Mars. *Sedimentology*, **64**, 311–358.

Stack, K.M. and Grotzinger, J.P. (2015) Constraining the Relative Timing and Duration of an Ancient Fluvio-Lacustrine System in Gale Crater Using MSL Curiosity Rover Observations. Presented at the Lunar and Planetary Science Conference, p. 2012. 46th Lunar and Planet. Sci. Conf., abstract 2012.

Summons, R.E., Amend, J.P., Bish, D., Buick, R., Cody, G.D., Des Marais, D.J., Dromart, G., Eigenbrode, J.L., Knoll, A.H. and Sumner, D.Y. (2011) Preservation of Martian organic and environmental records: final report of the Mars Biosignature working group. *Astrobiology*, **11**, 157–181.

Sumner, D.Y., Williams, R.M.E., Schieber, J., Palucis, M.C., Oehler, D.Z., Mangold, N., Kah, L.C., Gupta, S., Grotzinger, J.P., Grant, J.A., Edgar, L.A. and Dietrich, W.E. (2015) Fluvial to Lacustrine Facies Transitions in Gale Crater, Mars. Presented at the 2015 Joint Assembly, Montreal, Canada, May 3–7, 20150003056.

Thomson, B.J., Bridges, N.T., Milliken, R., Baldridge, A., Hook, S.J., Crowley, J.K., Marion, G.M., de Souza Filho, C.R., Brown, A.J. and Weitz, C.M. (2011) Constraints on the origin and evolution of the layered mound in Gale Crater, Mars using Mars Reconnaissance Orbiter data. *Icarus*, **214**, 413–432.

Vaniman, D.T., Bish, D.L., Ming, D.W., Bristow, T.F., Morris, R.V., Blake, D.F., Chipera, S.J., Morrison, S.M., Treiman, A.H., Rampe, E.B., Rice, M., Achilles, C.N., Grotzinger, J.P., McLennan, S.M., Williams, J., Bell, J.F., Newsom, H.E., Downs, R.T., Maurice, S., Sarrazin, P., Yen, A.S., Morookian, J.M., Farmer, J.D., Stack, K.,

Milliken, R.E., Ehlmann, B.L., Sumner, D.Y., Berger, G., Crisp, J.A., Hurowitz, J.A., Anderson, R., Des Marais, D.J., Stolper, E.M., Edgett, K.S., Gupta, S. and **Spanovich, N.** (2014) Mineralogy of a Mudstone at Yellowknife Bay, Gale Crater, Mars. *Science*, **343**, 1243480.

Vasavada, A.R., Grotzinger, J.P., Arvidson, R.E., Calef, F.J., Crisp, J.A., Gupta, S., Hurowitz, J., Mangold, N., Maurice, S., Schmidt, M.E., Wiens, R.C., Williams, R.M.E. and **Yingst, R.A.** (2014) Overview of the Mars Science Laboratory mission: Bradbury Landing to Yellowknife Bay and beyond. *J. Geophy. Res. Planets*, **119**, 1134–1161.

Wiens, R.C., Maurice, S., Barraclough, B., Saccoccio, M., Barkley, W.C., Bell III, J.F., Bender, S., Bernardin, J., Blaney, D., Blank, J., Bouye, M., Bridges, N., Bultman, N., Cais, P., Clanton, R.C., Clark, B., Clegg, S., Cousin, A., Cremers, D., Cros, A., DeFlores, L., Delapp, D., Dingler, R., D'Uston, C., Dyar, M.D., Elliott, T., Enemark, D., Fabre, C., Flores, M., Forni, O., Gasnault, O., Hale, T., Hays, C., Herkenhoff, K., Kan, E., Kirkland, L., Kouach, D., Landis, D., Langevin, Y., Lanza, N., LaRocca, F., Lasue, J., Latino, J., Limonadi, D., Lindensmith, C., Little, C., Mangold, N., Manhes, G., Mauchien, P., McKay, C., Miller, E., Mooney, J., Morris, R.V., Morrison, L., Nelson, T., Newsom, H., Ollila, A., Ott, M., Pares, L., Perez, R., Poitrasson, F., Provost, C., Reiter, J.W., Roberts, T., Romero, F., Sautter, V., Salazar, S., Simmonds, J.J., Stiglich, R., Storms, S., Striebig, N., Thocaven, J.-J., Trujillo, T., Ulibarri, M., Vaniman, D., Warner, N., Waterbury, R., Whitaker, R., Witt, J. and **Wong-Swanson, B.** (2012) The ChemCam instrument suite on the Mars Science Laboratory (MSL) rover: body unit and combined system tests. *Space Sci. Rev.*, **170**, 167–227.

Williams, R.M.E., Grotzinger, J.P., Dietrich, W.E., Gupta, S., Sumner, D.Y., Wiens, R.C., Mangold, N., Malin, M.C., Edgett, K.S., Maurice, S., Forni, O., Gasnault, O., Ollila, A., Newsom, H.E., Dromart, G., Palucis, M.C., Yingst, R.A., Anderson, R.B., Herkenhoff, K.E., Le Mouélic, S., Goetz, W., Madsen, M.B., Koefoed, A., Jensen, J.K., Bridges, J.C., Schwenzer, S.P., Lewis, K.W., Stack, K.M., Rubin, D., Kah, L.C., Bell, J.F., Farmer, J.D., Sullivan, R., Van Beek, T., Blaney, D.L., Pariser, O. and **Deen, R.G.** (2013) Martian fluvial conglomerates at gale crater. *Science*, **340**, 1068–1072.